

Journal of Geophysical Research: Atmospheres

RESEARCH ARTICLE

10.1002/2016JD025799

Key Points:

- TGF production appears to closely follow when/where lightning occurs in tropical storm systems
- Characteristics of TGFs from tropical storm systems appear similar to those produced by other storms
- TGF/sferic ratios may imply a high efficiency of TGF generation from lightning in some storms

Correspondence to:O. J. Roberts,
oliver.roberts@nasa.gov**Citation:**

Roberts, O. J., G. Fitzpatrick, G. Priftis, K. Bedka, T. Chronis, S. McBreen, M. S. Briggs, E. Cramer, B. Mailyan, and M. Stanbro (2017), Terrestrial gamma-ray flashes due to particle acceleration in tropical storm systems, *J. Geophys. Res. Atmos.*, 122, 3374–3395, doi:10.1002/2016JD025799

Received 17 AUG 2016

Accepted 30 JAN 2017

Accepted article online 1 FEB 2017

Published online 16 MAR 2017

Terrestrial gamma ray flashes due to particle acceleration in tropical storm systems

O. J. Roberts¹ , G. Fitzpatrick^{1,2}, G. Priftis³ , K. Bedka⁴ , T. Chronis³, S. McBreen¹ , M. S. Briggs², E. Cramer² , B. Mailyan² , and M. Stanbro² 

¹School of Physics, University College Dublin, Belfield, Ireland, ²CSPAR, University of Alabama in Huntsville, Huntsville, Alabama, USA, ³ESSC, University of Alabama in Huntsville, Huntsville, Alabama, USA, ⁴NASA Langley Research Center, Hampton, Virginia, USA

Abstract Terrestrial gamma ray flashes (TGFs) are submillisecond flashes of energetic radiation that are believed to emanate from intracloud lightning inside thunderstorms. This emission can be detected hundreds of kilometers from the source by space-based observatories such as the Fermi Gamma-ray Space Telescope (Fermi). The location of the TGF-producing storms can be determined using very low frequency (VLF) radio measurements made simultaneously with the Fermi detection, allowing additional insight into the mechanisms which produce these phenomena. In this paper, we report 37 TGFs originating from tropical storm systems for the first time. Previous studies to gain insight into how tropical cyclones formed and how destructive they can be include the investigation of lightning flash rates and their dependence on storm evolution. We find TGFs to emanate from a broad range of distances from the storm centers. In hurricanes and severe tropical cyclones, the TGFs are observed to occur predominately from the outer rainbands. A majority of our sample also show TGFs occurring during the strengthening phase of the encompassing storm system. These results verify that TGF production closely follows when and where lightning predominately occurs in cyclones. The intrinsic characteristics of these TGFs were not found to differ from other TGFs reported in larger samples. We also find that some TGF-producing storm cells in tropical storm systems far removed from land have a low number of WWLN sferics. Although not unique to tropical cyclones, this TGF/sferic ratio may imply a high efficiency for the lightning in these storms to generate TGFs.

1. Introduction

Terrestrial gamma ray flashes (TGFs) were a serendipitous discovery by the Burst And Transient Source Experiment (BATSE) on board the Compton Gamma Ray Observatory in 1994 [Fishman *et al.*, 1994]. These bursts of gamma ray radiation are characterized by their hard energy spectra (up to tens of MeV) [e.g., Smith *et al.*, 2005; Briggs *et al.*, 2010; Tavani *et al.*, 2011], and short (≤ 1 ms) timescale [Gjesteland *et al.*, 2010; Briggs *et al.*, 2013; Fitzpatrick *et al.*, 2014; Foley *et al.*, 2014]. TGFs have been studied extensively by space missions from low-Earth orbit, such as the Reuven Ramaty High Energy Solar Spectroscopic Imager (RHESSI) [Grefenstette *et al.*, 2009], Astrorivelatore Gamma a Immagini LEggero (AGILE) [Marisaldi *et al.*, 2014], and the Gamma-ray Burst Monitor (GBM) [Briggs *et al.*, 2013] and Large Area Telescope (LAT) [Grove *et al.*, 2012] on board the Fermi Gamma-ray Space Telescope.

In order to generate energy spectra up to tens of MeV, it is widely accepted that TGFs are produced via bremsstrahlung from the acceleration of high-energy electrons in the electric fields of thunderstorms. More on this bremsstrahlung process can be found in a review article by Dwyer *et al.* [2012]. Although the exact generation mechanism behind the production of TGFs is still ambiguous, three leading models have emerged: one involving the Relativistic Feedback Discharge (RFD) model and two that are based on different conditions involving the lightning leader tip model. The former is a self-sustained production of relativistic runaway electron avalanches (RREA), which results in a rapid burst of gamma rays [Dwyer, 2008, 2012]. The latter involves either a model in which seed electrons are created in the leader tip, but RREA takes place in a large-scale electric field [Moss *et al.*, 2006; Dwyer, 2012], or a model in which both the seed production and RREA take place in lightning leader field [Celestin and Pasko, 2011; Babich *et al.*, 2015].

Although initially thought to originate from high-altitude discharges associated with Sprites, subsequent measurements later determined that TGFs were produced at source altitudes below 30 km [Cummer *et al.*, 2005; Carlson *et al.*, 2007; Dwyer, 2008]. TGF energy spectra were also found to be consistent with production occurring at a source altitude of ~ 15 km [Dwyer and Smith, 2005]. Other studies of the gamma ray attenuation [Williams *et al.*, 2006; Fitzpatrick *et al.*, 2014], spectral shape [Carlson *et al.*, 2007; Østgaard *et al.*, 2008; Gjesteland *et al.*, 2010], and meteorology [Chronis *et al.*, 2015; Gjesteland *et al.*, 2015; Fabró *et al.*, 2015] have also confirmed that TGFs are produced from thunderstorms with a wide range of convective strengths [Chronis *et al.*, 2015], but predominately at an altitude between 10 and 16 km. The study by [Chronis *et al.*, 2015] also reported a TGF (oTGF130606592) which originated from the rainband of tropical storm Andrea, which is also reported in this study.

This paper will expand upon these previous meteorological studies by examining a sample of TGFs from tropical storm systems for the first time, in particular, whether TGFs from tropical storms are different from other TGFs and whether this sample of TGFs can reveal anything about how TGFs are produced. The implications of lightning activity at different storm phases on TGF production will also be discussed.

A general overview of the electrification in tropical storms and previous studies of lightning rates in tropical storm systems is given in section 2. Section 3 discusses the instrumentation and methods used in the analysis of the results in this paper. Section 4 will present the final TGF sample. Each of the TGFs in this sample was identified in tropical storms using satellite imagery data, correlated with VLF radio measurements. The gamma ray properties of these TGFs were calculated and compared to a larger TGF sample published in the literature. Section 5 reports on the results of the TGFs found in this paper, and their implications on our understanding of the generation of TGFs in hostile meteorological environments.

2. Electrification in Tropical Storms

A tropical storm is a storm system characterized by a low-pressure center with a closed circulation of strong winds, surrounded by thunderstorms in a spiral arrangement. These storms are referred to as a tropical depression, tropical storm, hurricane, typhoon, or a cyclone and are categorically classified according to their location and speed, taken as either a 1 min or 10 min average at a standard reference height of 10 m. In this paper, we categorize these storms according to their velocity over a 1 min average as the following; tropical depression ($17 \text{ m s}^{-1} \leq v_{\max}$), tropical storm ($18 \text{ m s}^{-1} \leq v_{\max} \leq 32 \text{ m s}^{-1}$) or a hurricane/typhoon/cyclone ($v_{\max} \geq 33 \text{ m s}^{-1}$). Some TGFs in this data occur in tropical low systems (areas of convection which do not show circulation), which later form or are the remnants of named storms.

Lightning has been shown to be infrequent in hurricanes, when compared to continental storm systems [Cecil *et al.*, 2002; Cecil and Zipser, 2002]. This is particularly true for macroscopic storm systems out in the open ocean, many hundreds of km from land. Due to the lack of sustained surface heating from the open ocean, the updrafts are weaker [Black *et al.*, 1996]. This results in fewer water droplets being transported aloft to above the freezing level, and less buoyancy in the thunderstorms that make up the inner rainbands of Hurricanes. These water droplets are key to creating charge separation, and therefore, their paucity contributes to the low lightning activity around the center of hurricanes [Cecil *et al.*, 2002; Cecil and Zipser, 2002]. The horizontal winds resulting from the rapidly rotating cores in Hurricanes cause the ice crystals to splinter below and above the freezing layer, creating very small ice crystals. The few supercooled water droplets that exist due to the weak updrafts in the subfreezing layers of the storm will quickly diffuse into the shards of small ice crystals [Fitzpatrick, 2006]. Lightning is therefore more common in the outer core of hurricanes where stronger updrafts occur due to greater cloud buoyancy. For an intensifying storm, however, the inner core can still experience a burst of electrical activity. Molinari *et al.* [1999] found that for several major hurricanes, unusually tempestuous eyewall thunderstorms are associated with sudden storm intensification, since lightning is dependent on the strength of the updraft.

Nagele [2010] studied cloud-to-ground (CG) lightning activity detected by the National Lightning Detection Network (NLDN) within Atlantic hurricanes. Like previous studies, they reported that lightning flashes were primarily detected in the rainbands for stronger storms. However, they also found that weaker hurricanes generated more lightning flashes within the inner core region and additionally observed that there was a strong correlation between lightning activity within this region and the minimum sea level pressure for 12 of the 16 hurricanes in the sample. Zhang *et al.* [2012] performed a similar study for tropical storms in the northwest Pacific Ocean using the Guandong Lightning Location System [Chen *et al.*, 2004]. In this study,

radial distribution of lightning was found to be dependent on the intensity of the storm system. For tropical storms with $17.2 \text{ m s}^{-1} \leq v_{\max} \leq 32.6 \text{ m s}^{-1}$, the ratio of the lightning density between the eyewall and the outer rainbands was 1:0.5, which decreased to 1:2.9 for typhoons ($32.7 \leq v_{\max} \leq 41.4 \text{ m s}^{-1}$) and 1:8.6 for severe typhoons ($41.5 \leq v_{\max} \leq 50.9 \text{ m s}^{-1}$) [Zhang et al., 2012].

Studies of thunderstorms that occur over land find that the sum of CG and intracloud (IC) strikes (total lightning) are well correlated with updraft speed and thunderstorm convection structure [Wiens et al., 2005]. Total lightning has also been used to probe the convective evolution and intensity of tropical storms [De Maria et al., 2012; Bovalo et al., 2014]. Fierro et al. [2011] used data from LASA (Los Alamos Sferic Array) [Shao et al., 2006] to study the rapid intensification of Hurricanes Rita, Katrina, and Charley. Using this limited-area lightning network that detects both CG and intense IC discharges, they observed an increase in the discharge heights of highly energetic IC flashes that were associated with convective bursts and strengthening updrafts.

3. Observations and Data

The TGFs in this paper were detected by the Gamma-ray Burst Monitor (GBM), one of two instruments aboard the Fermi Gamma-ray Space Telescope (hereafter referred to as Fermi for the remainder of the paper). Fermi GBM consists of 14 scintillator detectors; 12 thallium-doped sodium iodide (NaI:Tl) detectors, and 2 bismuth germanate (BGO) detectors [Meegan et al., 2009]. The NaI:Tl detectors are arranged in clusters of three, around each corner of the spacecraft and have dimensions of $\phi 12.7 \text{ cm} \times 1.27 \text{ cm}$, where ϕ is the diameter of the crystal. The BGO detectors are positioned on two opposing sides of the spacecraft and have dimensions of $\phi 12.7 \text{ cm} \times 12.7 \text{ cm}$. The effective area of one BGO detector was previously determined to be $\sim 161 \text{ cm}^2$ [Tierney et al., 2013]. The effective energy ranges of both the NaI:Tl and BGO detectors are about 8–1000 keV and 0.2–40 MeV, respectively. The large effective area, spectral range, and high timing resolution of both the NaI:Tl and BGO detectors allow for the individual study of each TGF due to the collection of sufficient statistics.

The orbit of Fermi allows for the detection of TGFs up to 25.6° north and south of the equator. In comparison, AGILE has an inclination of 2.5° , RHESSI has an inclination of 38° , and BATSE had an inclination of 28.5° . The NaI:Tl and BGO detectors are powered off during the spacecrafts transit through the South Atlantic Anomaly region due to the high particle activity.

Since its launch on 11 June 2008, Fermi-GBM has detected over 3300 TGFs up until 23 June 2015 (G. Fitzpatrick et al., in preparation at <https://fermi.gsfc.nasa.gov/ssc/data/access/gbm/tgf/>). These include both the TGFs that triggered GBM and those that were found by performing an off-line search using dedicated software. The off-line search program [Briggs et al., 2013] finds and analyzes short transients it identifies as being TGFs, suppressing cosmic rays, and data glitches. Team scientists perform additional manual screening to remove non-TGFs from the sample, which is followed by a further removal of cosmic rays using data from the Large Area Telescope (LAT) [Atwood et al., 2009].

The extremely luminous and short nature of TGFs results in large instrumental effects, such as dead time and pulse pileup [e.g., Grefenstette et al., 2008; Briggs et al., 2010; Tierney et al., 2013]. TGFs are detected in the GBM time-tagged event (TTE) data type, which has a relative temporal resolution of $2 \mu\text{s}$ and is made up of 128 pseudologarithmically spaced energy channels. The nominal dead time is $2.6 \mu\text{s}$; however, for events that are registered in the overflow channels of the NaI:Tl ($>1 \text{ MeV}$) and BGO detectors ($>40 \text{ MeV}$), the dead time is $10 \mu\text{s}$ [Meegan et al., 2009].

3.1. TGF Correlations With VLF Radio Measurements

It is believed that TGFs are produced during +IC lightning events [Stanley et al., 2006; Williams et al., 2006]. In the absence of a correlated radio measurement, the source location of a TGF detected by GBM is limited to a $\sim 800 \text{ km}$ region centered on the satellite nadir. However, with a radio measurement the true location can be known to an accuracy of $\sim 10 \text{ km}$. The radio signals detected simultaneously with the TGFs are likely to be dominated by emission related to the TGFs rather than the lightning processes. This was shown by Connaughton et al. [2013], who found a strong anti-correlation between TGF duration and the probability of a VLF radio detection by the WWLLN. As the TGF becomes longer, the frequency of the radio emission moves out of the WWLLN passband [Dwyer and Cummer, 2013]. VLF signals associated with TGFs are critical because they provide more accurate source localizations [Inan et al., 1996; Cummer et al., 2005; Cohen et al., 2006; Connaughton et al., 2010, 2013; Collier et al., 2011].

To date, ~1300 TGFs detected by Fermi GBM have been correlated with VLF radio signals (G. Fitzpatrick et al., in preparation at <https://fermi.gsfc.nasa.gov/ssc/data/access/gbm/tgf/>). Data from two ground-based lightning location networks were used to localize TGFs to a particular storm in this sample: the World Wide Lightning Location Network (WWLLN) (<http://wwlln.net/>) and the Earth Networks Total Lightning Network (ENTLN) (<https://www.earthnetworks.com/networks/lightning/>).

The ENTLN has more than 800 wideband electrical field recorders (with a frequency from 1 Hz to 12 MHz), installed globally [Hutchins et al., 2013]. Pulses in the electric field are located by time of arrival and subsequently grouped into flashes. The focus of the network has been on detecting IC flashes from continental storms for thunderstorm monitoring applications, as IC lightning is strongly correlated with storm intensity and generally precedes severe weather events, such as tornadoes [Liu and Heckman, 2011; Rudlosky, 2015]. More on the detection efficiency of ENTLN relative to Lightning Imaging Sensor (LIS) can be found in Rudlosky [2015] and on the ENTLN website.

The WWLLN detects VLF radio waves over a range of about 3–30 kHz, emitted by CG and a non-negligible fraction of IC lightning strokes. Significant radiated electromagnetic power exists from a few hertz to several hundred megahertz, with the bulk of the energy radiated at VLF. The WWLLN provides estimates of the time and location of global lightning strikes through the analysis of the energy of VLF electromagnetic events (sferics), measured by the ground stations. The location of the lightning strikes is determined using the “time of group arrival,” similar to that used for the ENTLN [Dowden et al., 2002]. The ground stations can be separated by thousands of kilometers because the VLF frequencies can propagate within the Earth-ionosphere waveguide with little attenuation [Price, 2008]. The WWLLN started off operations with 11 sensors from 2003 [Lay et al., 2004], which steadily increased to more than 70 sensors by the beginning of 2013 [Hutchins et al., 2013]. From 2008, the WWLLN detection efficiency relative to the New Zealand Lightning Detection Network (NZLDN) was 63% [Rodger et al., 2008]. Modeling studies using LASA [Rodger et al., 2005; Jacobson et al., 2006] and other more accurate networks estimate the WWLLN localization accuracy to be ~15 km.

The WWLLN detection efficiency for both CG and IC strokes is similar, providing the peak current of the two is comparable [Lay et al., 2004; Jacobson et al., 2006; Abarca et al., 2010]. WWLLN only detects strokes with peak currents ≥ 30 kA, and therefore, since CG strikes typically have higher peak currents than IC strikes, the network primarily detects the former [Virts et al., 2013]. The WWLLN has a higher detection efficiency over the ocean, as the peak currents of flashes over the oceanic regions are generally larger and therefore easier to detect remotely [Seity et al., 2001; Said et al., 2013; Virts et al., 2013]. Therefore, the WWLLN is well suited to tropical storm studies due to its global coverage and its ability to detect both IC and CG lightning. A comparative performance study of the ENTLN and WWLLN can be found in Bui et al. [2015].

Total lightning measurements can also be measured from satellites. The Optical Transient Detector (OTD) provided total lightning data from 1995 to 2002, and the Lightning Imaging Sensor (LIS) on the Tropical Rainfall Measuring Mission (TRMM) satellite continuously provided lightning data measurements up until 15 April 2015. Both the OTD and LIS were in low-Earth orbit and had small fields of view. Consequently, they measure the lightning from a storm over a period of only a few minutes, and therefore, we do not use these data to study the evolution of storm systems. There was also no TRMM data within 1 h for any of the TGF-producing storms in this sample, and therefore, we also exclude the use of this data.

For each of the TGFs in this sample, there is a confirmed VLF radio match from the WWLLN, ENTLN, or both. TGFs are screened by members of the TGF team and by the LAT, for short GRBs, SGRs, solar flares, time glitches, and cosmic rays. TGFs with more than one accepted location are averaged. TGFs that have two VLF localizations with separations that exceed 50 km are rejected. The match rate for correlating a radio sferic to a Fermi-GBM TGF is about 1 in 3 for the WWLLN data [Connaughton et al., 2013]. An updated value for the efficiency of radio associations correlated with TGFs from these networks can be found in G. Fitzpatrick et al. (in preparation at <https://fermi.gsfc.nasa.gov/ssc/data/access/gbm/tgf/>).

3.2. TGF Correlations With the Tropical Storm Data

The TGFs in this study are then correlated to tropical storm systems using imagery data from the Geostationary Operational Environmental Satellite (GOES) and the Multifunction Transport Satellite (MTSAT).

The GOES Imager covers five channels, one in the visible spectral range (0.55–0.75 μm), and four in the infra-red (IR) (3.8–4.0 μm , 6.5–7.0 μm , 10.2–11.2 μm , and 11.5–12.5 μm) (More information on GOES can be found here: <http://www.ospo.noaa.gov/Operations/GOES/>). The data came from GOES 11 to GOES 15, which

covered 240°–315° east longitude. Although some of the centered wavelengths in each of these channels changed slightly with the launch of GOES 12, all Channel 4 (10.2–11.2 μm) data was centered on 10.7 μm during the entire sample duration. The data was extracted and analyzed using the Space Physics Environment Data Analysis Software, an open-source data analysis tool written in IDL.

The MTSAT data came from MTSAT 1R [Puschell *et al.*, 2002; Uesawa, 2006] and MTSAT 2 [Uesawa, 2006], and covered a hemisphere centered on 140° east longitude. Both satellites provide imagery in five wavelength bands similar to GOES; one in the visible spectral range (0.55–0.80 μm) and four in the IR (3.5–4.0 μm, 6.5–7.0 μm, 11.5–12.5 μm, and 10.3–11.3 μm). The resolution of the IR data is 4 km (the resolution is lower as one moves away from the equator at 140° east). MTSAT was replaced by *Himawari-8* [Bessho *et al.*, 2016] on 7 July 2015. The high-resolution IR MTSAT data from 10.3 to 11.3 μm was used for the images of the West Pacific, South Pacific, and Indian Ocean storms presented in this paper.

In addition to the imagery data, the storm track history is taken from the National Oceanic and Atmospheric Administration (NOAA) data (<http://www.nhc.noaa.gov/data/>), Weather Underground's Hurricane Archive (<https://www.wunderground.com/hurricane/hurrarchive.asp>), and the UniSys archive (<http://weather.unisys.com/hurricane/>).

3.3. Gamma Ray Analysis

As the TTE data from GBM yields a large sample size of TGFs, an automatic technique is needed to characterize the temporal properties of each TGF [Fitzpatrick *et al.*, 2014], which is provided by the Bayesian Block Algorithm (BBA) [Scargle *et al.*, 2013]. The BBA divides the data into blocks, each block being consistent with a constant rate. The BBA addresses the problem of detecting and characterizing variability in the TTE data by finding the optimal segmentation or boundaries between the blocks, termed “change points.” The goal is to separate statistically significant, valid events from random observational errors using a nonparametric analysis of time.

The events were chopped from the TTE data and analyzed using a false-positive probability (p0) of 0.05, which was determined to be a good value to use from previous studies [Scargle *et al.*, 2013]. Once the source region was identified, the gamma ray properties are calculated. A pivot energy of 300 keV was used to determine the hardness ratio (HR) of each event.

4. Results

Table 1 shows a sample of 37 TGFs detected by GBM that are associated with organized tropical storm systems, which are mapped in Figure 1. The GBM sample was taken over a period of 7 years; from the launch of the spacecraft in 2008 until 31 December 2015. The TGFs are classified as tTGF or oTGF, depending on whether they triggered the GBM, or were found offline by the search program, respectively. The naming convention of the TGF follows the date code “YYMMDDXXX”, where “YY” are the two last digits of the year, “MM” is the month, and “DD” is the day of detection. Here “XXX” refers to the fraction of the day, which ranges from 000 to 999. The TGFs from the tropical storms in this sample are found to contribute a non-negligible fraction of oceanic TGFs, in addition to those TGFs produced as a result of storms from the Intertropical Convergence Zone (ITCZ) [Splitt *et al.*, 2010; Briggs *et al.*, 2013]. The TGF peak time is estimated using the TGF start time and half the discovery bin width, as determined by the off-line search program or the Fermi-GBM flight software. This estimated TGF peak time was then correlated with the lightning stroke from the VLF measurements to within ~200 μs, for 31 of the 37 TGFs in this sample. The remaining six are correlated to within ~3.5 ms. Table 1 shows the calculated distance between the correlated TGF-VLF event and the storm center. The east longitude and latitude of each storm-producing TGF was calculated using the near-simultaneous detection of VLF sferics in both the WWLN and ENTLN data. These associations were then correlated with tropical storm systems using imagery data from GOES and MTSAT. An additional six TGFs were possibly found to originate from storm cells in tropical storm systems but were excluded from the initial sample of 43 events, as they either lacked an association with a sferic or had no satellite imagery data within an hour on either side of the detection time.

Figure 2 is an image acquired from MTSAT for oTGF150708613, which covers a narrow passband wavelength of 10.2–11.2 μm and is temporally coincident to within 60 min of the TGF time. Satellite imagery acquired outside of this time window were rejected, as the convective dynamics of the storms in such an image would not be representative of the storm cell that produced the TGF.

Table 1. This Table Shows the TGFs in the Sample^a

TGF ID (YYMMDD)	Time (UTC)	TGF-VLF Location Latitude	East Longitude	Storm Center (UTC) Latitude	East Longitude	Distance (km)	Wind (m s ⁻¹)	Mean Temperature (°C)	Cloud Top Height (km)	Category
oTGF 00916059	01:25:33	276.51	23.24	269.90 (0000)	19.20 (0000)	818.8	18.0	-73	15.1	Tropical storm
oTGF 00926583	13:59:33	265.29	18.73	267.10 (1500)	17.40 (1500)	241.8	10.3	-71	16.1	Tropical low
oTGF 01009389 ^b	09:19:52	294.13	21.26	301.50 (0900)	29.20 (0900)	1152.0	38.6	-51	11.5	Hurricane ^b
tTGF 01012231	05:32:32	277.72	17.63	275.10 (0600)	17.20 (0600)	282.4	30.9	-69	14.9	Tropical storm
oTGF 01012443	10:38:16	278.52	18.68	274.60 (1200)	18.10 (1200)	418.3	33.4	-57	13.0	Hurricane I
tTGF 010125162	03:52:43	122.05	-18.22	121.80 (1200)	-17.40 (1200)	94.9	18.0	N/A	-	Tropical storm
oTGF 10217556	13:20:12	112.64	-23.38	102.50 (1200)	-26.50 (1200)	1082.0	25.7	N/A	-	Tropical storm
oTGF 10924662	15:53:02	303.26	17.06	304.00 (1500)	17.80 (1500)	113.7	23.2	-66	14.0	Tropical storm
oTGF 20706651	15:37:09	264.71	13.81	-	-	-	-	N/A	-	Tropical low
oTGF 20807526	12:37:04	120.34	22.81	122.80 (1200)	28.10 (1200)	637.9	30.9	N/A	-	Tropical storm
oTGF 20816335	08:02:10	116.44	24.14	115.70 (0600)	19.40 (0600)	532.6	30.9	N/A	-	Typhoon
tTGF 20823943	22:37:17	135.07	14.09	133.60 (2400)	21.00 (2400)	784.0	54.0	N/A	-	Typhoon
oTGF 20928134	03:13:15	251.62	21.59	-	-	-	-	-82	-	Tropical Low
oTGF 20928988	23:42:19	250.61	24.32	251.40 (2400)	23.80 (2400)	98.8	18.0	-67	14.0	Tropical storm
oTGF 120929059	01:24:23	251.47	25.34	251.40 (0000)	23.80 (0000)	171.9	18.0	-63	13.3	Tropical storm
tTGF 121023222	05:19:31	287.72	12.97	281.30 (0600)	12.90 (0600)	695.7	20.6	-83	13.8	Tropical storm
oTGF 130115502	12:03:14	79.53	-13.91	79.00 (1800)	-14.40 (1800)	79.0	18.0	N/A	-	Tropical storm
oTGF 130605669	16:02:55	274.43	21.29	273.50 (2200)	25.30 (2200)	456.0	18.0	-75	18.0	Tropical storm
oTGF 130606592	14:12:18	275.98	25.59	275.70 (1500)	28.20 (1500)	291.4	25.7	-75	N/A	Tropical storm
oTGF 130705135	03:14:25	257.93	18.15	259.20 (0600)	14.90 (0600)	385.9	20.6	-64	13.4	Tropical storm
oTGF 130913367	08:47:54	262.49	22.95	264.90 (1200)	19.30 (1200)	455.9	20.6	-71	15.5	Tropical storm
oTGF 130915566	13:34:52	256.45	17.35	256.60 (1200)	18.20 (1200)	98.6	30.9	-86	N/A	Tropical storm
oTGF 130916277	06:38:36	253.69	20.38	254.80 (0600)	20.40 (0600)	115.5	12.9	-78	17.4	Tropical depression
tTGF 130916490	11:45:36	264.07	20.04	262.20 (1200)	23.80 (1200)	460.7	28.3	-69	15.2	Tropical storm
oTGF 131001376	09:01:54	135.71	20.24	132.60 (0200)	14.00 (0200)	788.5	15.4	N/A	-	Tropical depression
tTGF 131024758	18:11:59	253.44	14.12	253.6 (1800)	14.80 (1800)	77.6	20.6	-76	16.1	Tropical storm
tTGF 131103273	06:33:10	249.07	19.28	250.00 (0600)	18.50 (0600)	130.3	18.0	-84	N/A	Tropical storm
oTGF 140701088	02:07:22	277.23	26.17	281.10 (0000)	27.70 (0000)	419.4	15.4	-58	13.0	Tropical depression
oTGF 140803355	08:31:38	245.05	17.30	-	-	-	-	-56	12.8	Tropical low
oTGF 140803356	08:31:57	244.42	17.11	-	-	-	-	-76	15.3	Tropical low
oTGF 140803425a	10:11:40	243.98	15.21	-	-	-	-	N/A	-	Tropical low
oTGF 140803425b	10:12:21	244.14	17.32	-	-	-	-	N/A	-	Tropical low
tTGF 140804347	08:19:41	240.54	13.92	242.30 (0600)	13.50 (0600)	196.2	18.0	-81	15.9	Tropical storm
oTGF 140916552	13:14:59	251.15	24.34	247.00 (1200)	28.10 (1200)	588.1	25.7	-77	17.4	Tropical storm
oTGF 141002298	07:09:45	254.46	21.55	253.90 (0900)	18.10 (0900)	388.1	18.0	-72	9.7	Tropical storm
oTGF 150708613	14:42:4	145.16	17.12	149.10 (1200)	15.90 (1200)	441.4	59.2	N/A	-	Typhoon
oTGF 151010496	11:53:46	70.50	15.64	69.40 (1200)	15.20 (1200)	127.7	18.0	N/A	-	Tropical storm

^aThe naming convention for each TGF follows that of the Fermi GBM TGF catalog (G. Fitzpatrick et al., in preparation at <https://fermi.gsfc.nasa.gov/sc/data/access/gbm/tgf/>) and is explained in detail in section 4. The location of the storm-producing cell in relation to the storm system and the storm category is also listed, along with the maximum sustained winds (1 min). The cloud top temperatures and heights of some of the storms are listed where available. N/A, not applicable.

^bTGF 101009389 originates from a storm cell in an isolated frontal band, over 800 km away from the center of weakening Hurricane Otto, as it is transitioning into an extratropical system.

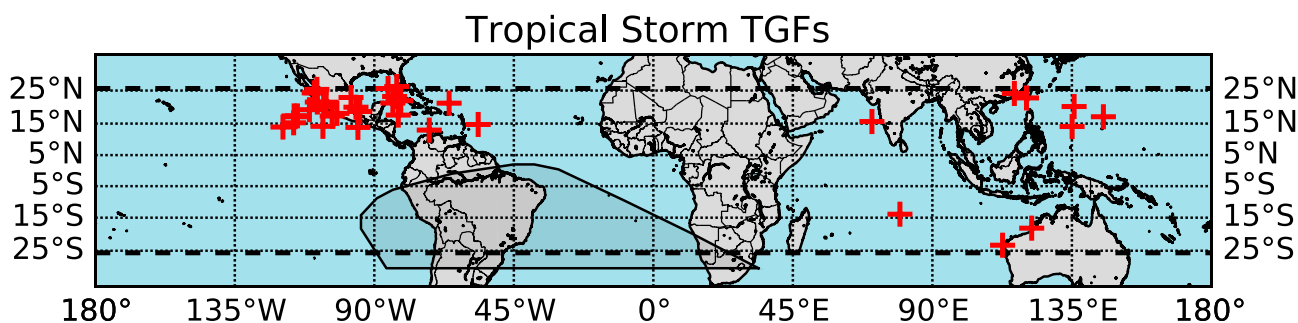


Figure 1. A map showing the global distribution of TGFs with correlated VLF sferics from the sample presented in this study. The dashed lines show the inclination of Fermi's orbit. The shaded region represents the location of the South Atlantic Anomaly.

Figures 3 and 4 show strokes from the VLF data over a 10 min period for two distinct storms, plotted with the GOES imagery. Figure 3 shows that the majority of the strokes (orange dots) can be found in the outer rainbands of Hurricane Paula, in the Gulf of Mexico. This correlates well with the anticipated lightning rates in tropical storm systems, based on previous studies [Cecil *et al.*, 2002; Cecil and Zipser, 2002]. Figure 4 shows strengthening Tropical Storm Sonia in the Eastern Pacific basin, with the VLF strokes strongly correlated to within ~100 km of the storm center.

The GOES data was used in addition to soundings acquired from ground stations positioned near a subset of the sample to calculate the mean cloud top height from the IR temperatures. The calculated temperatures and heights of the cloud tops for some of the events in this study can be found in Table 1. In some cases, the temperatures provided in the table were too low and did not correspond to any heights provided by the sounding, possibly due to the sounding being acquired too far from the location and/or time of the event (soundings are only available at 0000 and 1200 UTC). These temperatures are therefore not representative of the storm cell that produced the TGF. In some other cases, no sounding data were available. The estimated

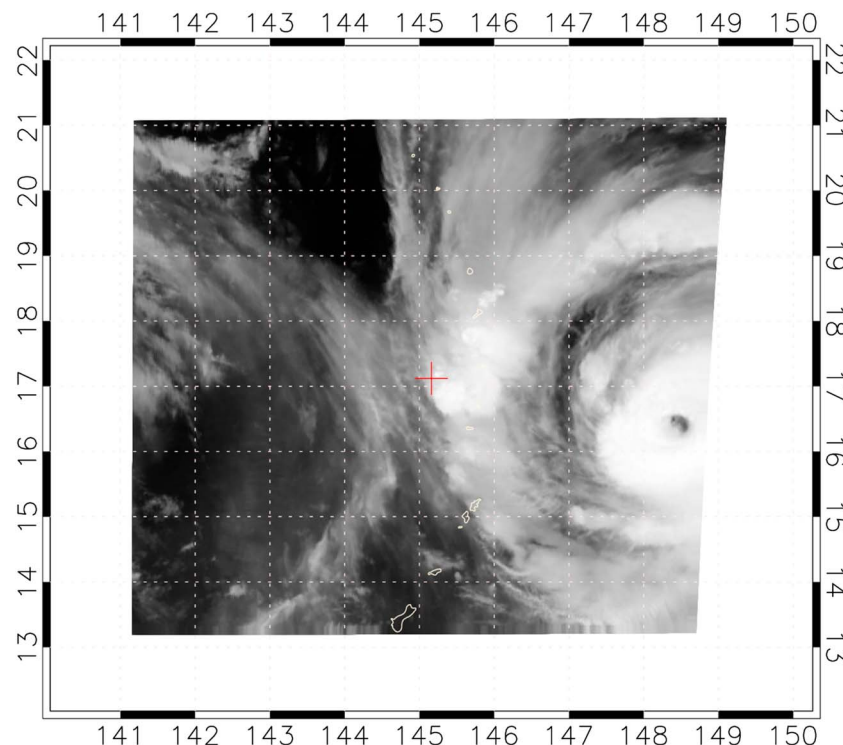


Figure 2. TGF150708613: The red cross represents the VLF source location (longitude: 145.16°E, latitude: +17.12°N), which was correlated with the GBM-detected TGF. The correlated TGF-VLF location was ~441 km from the center of Typhoon Nangka at the time of the TGF event.

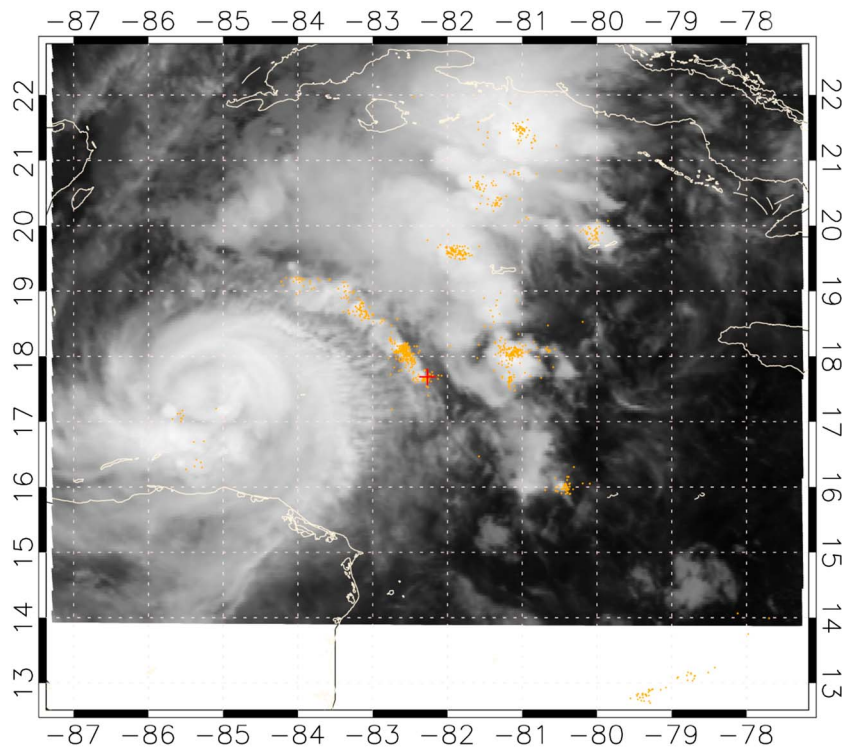


Figure 3. TGF101012231: The red cross represents the VLF source location (longitude: 277.72°E , latitude: $+17.63^{\circ}\text{N}$), which was correlated with the GBM-detected TGF. The orange dots represent the lightning strokes within 10 min of the TGF trigger. The correlated TGF-VLF location was ~ 282 km from the center of Category I Hurricane Paula at the time of the TGF event.

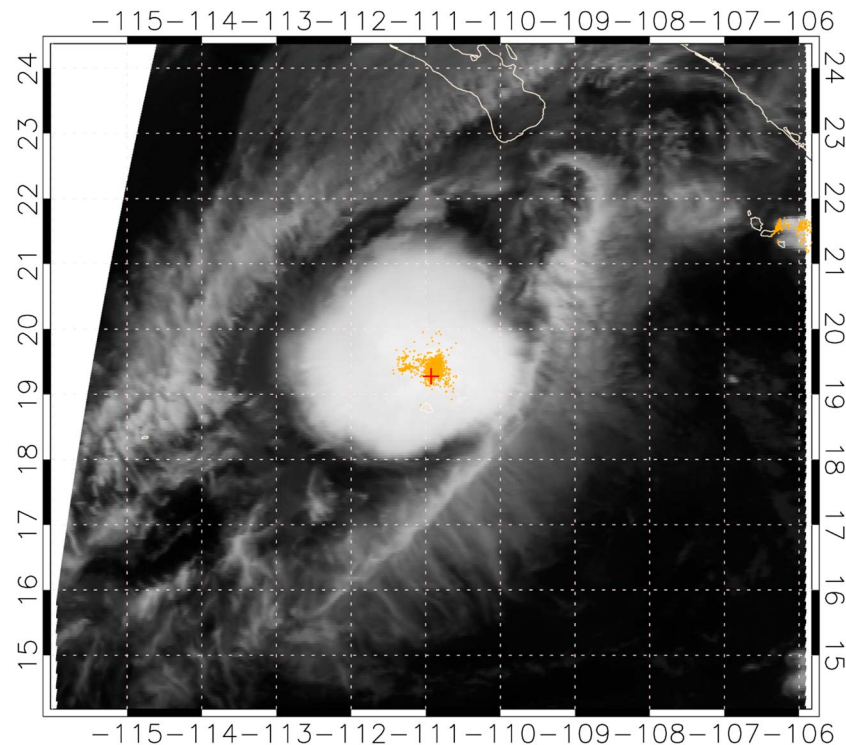


Figure 4. TGF131103273: The red cross represents the VLF source location (longitude: 249.07°E , latitude: $+19.28^{\circ}\text{N}$), which was correlated with the GBM-detected TGF. The orange dots represent the lightning strokes within 10 min of the TGF trigger. The correlated TGF-VLF location was ~ 130 km from the center of Tropical Storm Sonia at the time of the TGF event.

Table 2. The Spectral and Temporal Characteristics of the TGFs From the Sample as Determined by the Bayesian Analysis Presented in This Paper

TGF ID	Width (μs)	P2	LST	Delay (μs)	Delay Error (μs)	HR Error	t_{BB} (μs)
oTGF100916059	200.0	5.8E-23	0.833	42.3	15.9	0.68	0.21
oTGF100926583	100.0	8.6E-38	0.321	3.7	9.2	1.19	0.35
oTGF101009389	141.0	9.1E-43	0.210	17.2	9.5	0.45	0.11
tTGF101012231	283.0	2.7E-279	0.009	65.5	2.5	1.07	0.14
oTGF101012443	141.0	3.4E-81	0.222	74.9	4.4	0.55	0.11
tTGF110125162	283.0	9.8E-305	0.487	47.6	2.4	1.00	0.12
oTGF110217556	141.0	1.7E-73	0.851	34.1	6.1	1.02	0.22
oTGF110924662	70.7	1.3E-73	0.510	34.8	4.7	0.53	0.11
oTGF120706651	141.0	6.8E-63	0.387	37.6	5.7	0.67	0.15
oTGF120807526	200.0	1.0E-22	0.863	-19.0	20.9	1.26	0.35
oTGF120816335	100.0	3.8E-73	0.648	28.5	5.0	0.78	0.17
tTGF120823943	283.0	2.1E-134	0.318	39.1	5.9	1.95	0.36
oTGF120928134	141.0	2.7E-161	0.838	53.3	2.6	0.88	0.15
oTGF120928988	70.7	3.0E-46	0.695	-2.7	6.5	0.88	0.25
oTGF120929059	141.0	8.2E-77	0.771	45.0	6.2	1.10	0.24
tTGF121023222	283.0	2.5E-93	0.031	30.1	8.6	2.41	0.51
oTGF130115502	200.0	4.4E-72	0.704	-20.1	7.2	0.74	0.15
oTGF130605669	141.0	1.7E-58	0.439	22.6	6.7	1.13	0.28
oTGF130606592	283.0	8.2E-125	0.358	32.7	7.0	1.67	0.29
oTGF130705135	200.0	2.4E-80	0.836	72.2	6.3	0.91	0.19
oTGF130913367	141.0	4.8E-31	0.103	43.7	19.6	1.18	0.34
oTGF130915566	70.7	1.8E-52	0.291	1.7	8.9	1.09	0.32
oTGF130916277	141.0	8.0E-50	0.998	89.6	7.6	0.91	0.22
tTGF130916490	200.0	9.6E-292	0.230	30.8	3.8	2.40	0.35
oTGF131001376	200.0	6.8E-63	0.760	58.0	8.6	0.49	0.11
tTGF131024758	200.0	4.3E-207	0.470	89.8	2.7	0.71	0.10
tTGF131103273	283.0	6.0E-175	0.980	24.3	5.6	1.71	0.25
oTGF140701088	141.0	4.1E-116	0.860	35.6	5.2	1.22	0.23
oTGF140803355	200.0	1.5E-115	0.037	74.5	2.7	0.36	0.07
oTGF140803356	200.0	5.6E-95	0.040	41.0	5.5	0.41	0.09
oTGF140803425a	141.0	5.7E-21	0.085	-33.3	15.4	0.51	0.17
oTGF140803425b	200.0	1.9E-68	0.093	25.8	8.8	0.63	0.14
tTGF140804347	283.0	4.0E-299	0.008	10.5	2.7	1.57	0.20
oTGF140916552	141.0	1.9E-84	0.266	18.4	5.9	0.65	0.12
oTGF141002298	400.0	6.1E-76	0.006	21.6	8.8	1.16	0.22
oTGF150708613	200.0	0.0	0.023	88.6	2.7	0.65	0.09
oTGF151010496	141.0	0.0	0.694	79.9	2.7	0.65	0.09

cloud top heights provided in this study were all found to be ≥ 9.5 km, similar to values reported previously in *Chronis et al.* [2015]. Some of the cloud top heights are suggestive of some TGFs being produced from overshooting cloud tops, with altitudes of ≥ 17 km. However, such convective bursts are hard to resolve in the GOES and MTSAT data and tend to collapse on a short timescale (typically of the order of 10 to 60 min) [Bedka et al., 2015]. Higher-resolution data and analysis that are beyond the scope of this paper are required to verify these indications of overshooting cloud tops.

4.1. Gamma Ray Properties

Table 2 shows the results of the gamma ray analysis for the TGFs in the sample. In the table, “width” is the discovery bin width of the event as determined by the off-line search program [Briggs et al., 2013], “P2” is

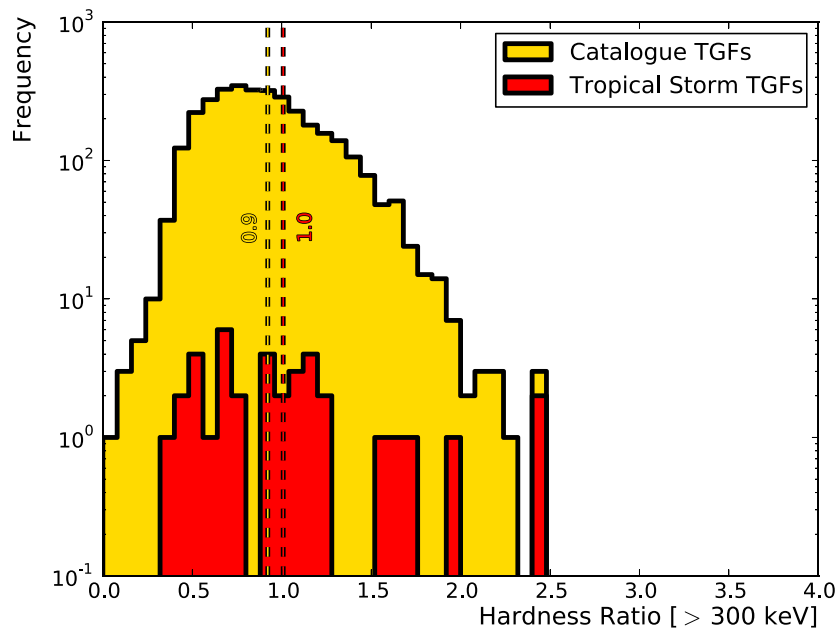


Figure 5. A distribution of the hardness ratio (HR) for each TGF from our sample (red) and from G. Fitzpatrick et al. (in preparation at <https://fermi.gsfc.nasa.gov/ssc/data/access/gbm/tgf/>) (yellow). The HR is defined as being the ratio of events with a photon energy >300 keV, divided by events ≤ 300 keV. The mean HR of both data sets are not shown to be significantly different (1.0 as opposed to 0.9).

the corrected, joint Poisson probability of the event [Briggs et al., 2013], “LST” is the local solar time as a fraction of a day, “Delay” is the delay between hard (>300 keV) and soft (<300 keV) events, “HR” is the ratio of hard events (>300 keV) to soft events (<300 keV), and “ t_{BB} ” is the duration of the TGF as determined by the BBA.

Figure 5 shows the hardness ratio (HR) of events from G. Fitzpatrick et al. (in preparation at <https://fermi.gsfc.nasa.gov/ssc/data/access/gbm/tgf/>) and from TGFs in this study. The average ratio of the spectral hardness

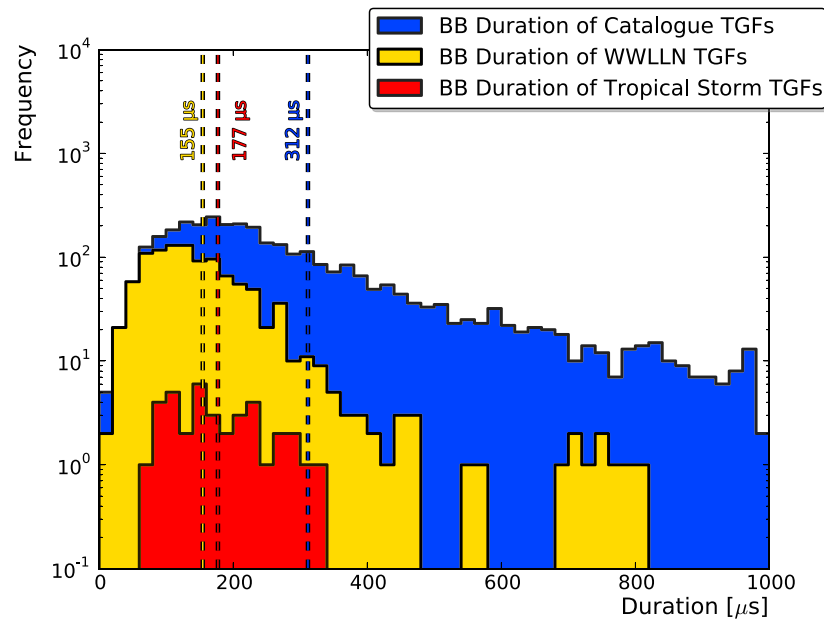


Figure 6. The TGF duration as determined by the Bayesian Block Algorithm (BBA) for all the TGFs in the release of the Fermi GBM TGF Catalog (blue), all TGFs from the same catalog release with a WWLLN association (yellow), and our sample (red). The dashed lines show the mean averages of each distribution.

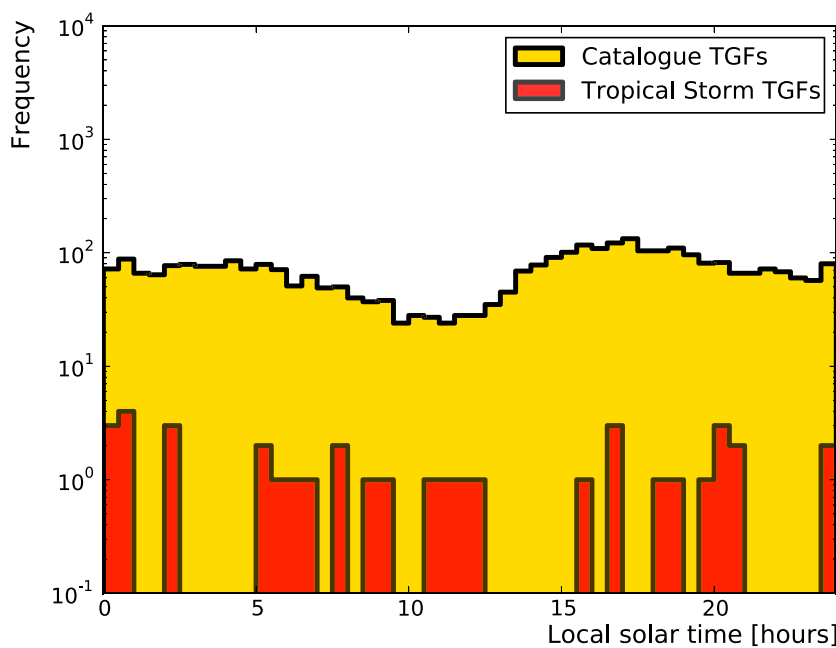


Figure 7. The distribution of TGFs from our sample (red) and from G. Fitzpatrick et al. (in preparation at <https://fermi.gsfc.nasa.gov/ssc/data/access/gbm/tgf/>) (yellow) for a Local Solar Time (LST), binned in half hour intervals.

of TGFs from both data sets shows no significant deviation. Figure 6 shows that the TGFs in Table 2 are short (<200 μ s) in comparison to the TGFs from G. Fitzpatrick et al. (in preparation at <https://fermi.gsfc.nasa.gov/ssc/data/access/gbm/tgf/>). The average duration (as determined by the Bayesian Block analysis), of the TGFs without a WWLLN association was found to be \sim 312 μ s, significantly longer when compared to the mean averages of other TGFs with a WWLLN association (\sim 155 μ s), and the events in our sample (\sim 177 μ s). This verifies previous findings that the association rate between TGFs and lightning strokes has a strong dependence on the TGF duration, with the shortest TGFs having a much higher association rate [Connaughton et al., 2013]. The latter distribution is not representative of all TGFs from tropical storm systems, just those with a WWLLN association. Figure 7 shows the distribution of TGFs from this study comparatively with TGFs taken from G. Fitzpatrick et al. (in preparation at <https://fermi.gsfc.nasa.gov/ssc/data/access/gbm/tgf/>), at a Local Solar Time (LST). This figure is binned in half hour intervals and shows that TGF generation within tropical storms is independent of the LST. This is in agreement with oceanic lightning rates, which are almost uniform with respect to LST [Christian et al., 2003; Blakeslee et al., 2014; Hutchins et al., 2014]. Other results of the BBA over the sample are given in Table 2. It appears that the TGFs from this study are consistent with the TGFs from the GBM catalog (G. Fitzpatrick et al., in preparation at <https://fermi.gsfc.nasa.gov/ssc/data/access/gbm/tgf/>).

5. Discussion

This study has so far shown that TGFs can be produced from storm cells in tropical storm systems and that their properties do not seem to behave differently from conventional TGFs. This section will investigate whether the TGFs in this paper are well-correlated to the anticipated lightning rates in tropical storms and whether TGF generation is dependent on the intensity and phase of the storm.

Table 1 shows the category of the storm during the time of the TGF event and an approximate distance from the storm center to the correlated TGF-VLF event. Of the 37 TGFs in this study, three are from tropical depressions ($17 \text{ m s}^{-1} \leq v_{\max}$), 22 are from tropical storms ($18 \text{ m s}^{-1} \leq v_{\max} \leq 32 \text{ m s}^{-1}$), and five are from hurricane/typhoon/cyclone systems ($v_{\max} \geq 33 \text{ m s}^{-1}$). The remaining are from tropical low systems, six of which intensify into a named system with $17 \text{ m s}^{-1} \leq v_{\max}$, and one of which is a remnant low, formed after the dissipation of a named storm. The reported storm center location is measured at varying time resolutions. For our sample, the position is available within 2 h of the TGF detection for all events with the exception of tTGF110125162, oTGF130115502, oTGF130605669, oTGF130913367, oTGF131001376, and oTGF150708613.

The seven TGFs which came from tropical low systems do not have storm center positions as they were not tracked at that time.

All five correlated TGF-VLF events from hurricanes/typhoons came from storm cells in their outer rainbands, far from the center of the storm. oTGF101009389 was found to originate from a storm cell in an isolated frontal band, over 800 km away from the center of weakening Hurricane Otto. As the TGF occurred during the transition of the storm into an extratropical system and is very far removed from the storm center, it is not discussed comparatively with other TGFs in this study.

Of the 22 correlated TGF-VLF events from tropical storms, oTGF120928988 and tTGF131024758 came from storm cells within 100 km of the center of the storm system and 30 min of the registered storm center position. Another three of the 22 events, oTGF110924662, oTGF130916227, and tTGF131103273, came from storm cells within 150 km of the center of the storm and 1 h of the registered storm center position. Figure 4 is a satellite image of Tropical Storm Sonia in the Eastern Pacific basin, taken within an hour of tTGF131103273. The TGF from this storm likely came from an overshooting cloud top, with an altitude of ≥ 17 km. This altitude is slightly higher than the altitude reported in *Mailyan et al. [2016]*, which was determined from fitting the energy spectrum of this TGF with an RREA model. Even though an RREA model of a narrow beam profile and source altitude of 16 km was found to be the best fit in that study to tTGF131103273, the likelihood difference was too small to convincingly reject other models that had a different beam profile or altitude. TGFs are known to originate below the cloud tops, in between the main negative and upper positive layers [*Dwyer et al., 2012*], so the lower altitude reported in the *Mailyan et al. [2016]* is still consistent with the findings in this paper.

5.1. Storm Phase Correlation

The storm phase of each tropical system in this paper was studied, in order to ascertain whether this effect has any direct influence on the rate of TGF production. Of the 37 TGFs studied, 25 were found to originate from a storm cell in an intensifying tropical system and 8 from a storm cell in a dissipating system. The remaining four were found to occur while the tropical system was at its peak intensity. An intensifying or strengthening storm is defined as an increase in the maximum sustained velocity (MSV) over a 1 min period of $\geq 2.6 \text{ m s}^{-1}$, or as a decrease in the minimum central pressure (MCP) of $\geq 1 \text{ mb}$, over a period of 6 h on either side of the TGF detection. Similarly, a dissipating or weakening storm is defined as a decrease in the MSV of $\geq 2.6 \text{ m s}^{-1}$, or increase in the MCP of $\geq 1 \text{ mb}$, within the same time window. The peak intensity of a storm system is where there are no changes in the MSV or MCP over a 6 h period. Figures 8 and 9 show the occurrence of 10 TGFs during the histories of nine strengthening tropical storm systems and 8 TGFs during the histories of six dissipating storm systems, respectively.

Figure 10 is another example of a strengthening tropical storm system. Tropical system Paula was intensifying as two TGFs, separated by approximately 5 h, were observed in the GBM data. Approximately 700 and 200 sferics were detected by the WWLLN within 10 min and 300 km of TGF-VLF associations tTGF101012231 and oTGF101012443, respectively. *Price [2009]* found a relationship between lightning activity and storm intensity using the WWLLN data, as well as a strong correlation between the maximum sustained wind speed and the total flash rate, with a maximum of lightning activity occurring about 30 h prior to maximum intensity. A study of several major Hurricanes in the Atlantic basin by *Fierro et al. [2011]* found that increases in the discharge heights of highly energetic IC flashes are associated with convective bursts and strengthening updrafts. The peak currents measured in that study are of the order of 20–30 kA. Although the ENTLN and the WWLLN detect a mixture of CG and IC lightning, the fraction of IC lightning events from both networks is always less. Only highly energetic IC events with peak currents comparable to or higher than CG lightning are recorded. *Connaughton et al. [2013]* reported a sample of sferics simultaneous with TGFs, to have currents comparable to CG lightning despite being +IC lightning. This bias to higher peak current events from both networks (but particularly for the WWLLN [*Rodger et al., 2006*]) suggests that the IC flashes that produced the TGFs from the storm systems in this paper may be due to convective bursts as a result of strengthening updrafts.

The strong correlation found here between the TGFs in this sample and the strengthening phase of storm systems needs to be interpreted carefully. A TGF from a tropical depression system does not mean that system will evolve into a major Hurricane later in the storm's lifetime. Many additional environmental parameters that are influential to how a tropical storm system evolves are not treated carefully enough in this study to make a definitive conclusion. More analysis and modeling is needed to verify this claim, along with a larger data sample.

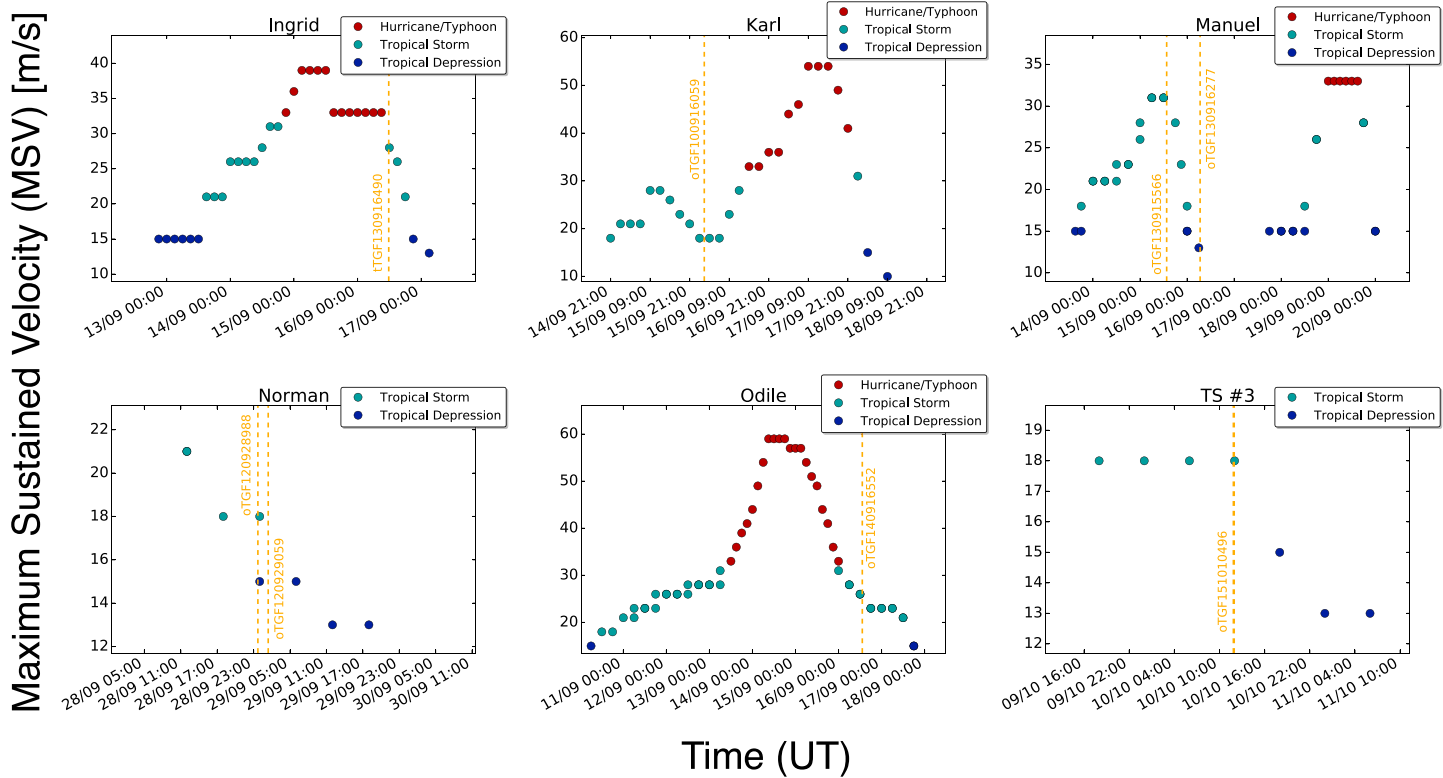


Figure 8. Storm histories of nine strengthening tropical storm systems, whose storm cells produced TGFs.

5.2. Storm Convection and Sferics

The number of sferics depends on the updraft strength of the storm and the efficiency of the VLF network. In this study, some storms were found to produce a very low number of sferics within 1000 km and 10 min of the TGF and WWLLN association. A ratio of TGFs to the number of sferics may be used to imply a high efficiency of TGF generation from lightning in such storms. Due to the uneven detection efficiencies of the WWLLN and the ENTLN, and the inability of the ENTLN to accurately distinguish between CG and IC lightning discharges for deep oceanic storms, data from the WWLLN were used for the case studies of three storms that produced a low numbers of sferics. *Virts et al.* [2013] has shown that WWLLN is relatively better than LIS at detecting sferics over the open ocean compared to land and to a lesser extent, that the uniformity is pretty good over the ocean.

In this section, we present the data from several low-sferic producing storm cells from three tropical storm systems and later discuss the implications of this study in the context of TGF production.

5.2.1. Typhoon Bolaven

Figure 11 is a satellite image of the southeast quadrant of Typhoon Bolaven in the northwest Pacific basin, taken by MTSAT on 23 August 2012. Typhoon Bolaven formed in the Pacific Ocean as a tropical depression on 19 August and strengthened as a tropical storm on 21 August. The image shown in Figure 11 was taken during a period of intensification by the storm system. The calculated distance from the outer rainband containing the storm cell which produced the TGF to the storm center is ~ 784 km. The uncertainty on the location of this event is about 10 km, and the storm center position is accurate to within 1° (longitude and latitude, equivalent to ~ 110 km), correct at 1 h and 22 min after event tTGF120823943. The TGF-VLF position is 597 km from land. Figure 12 shows a scatterplot of the energy distribution several milliseconds before and after the TGF detection time. This event consists of four pulses over a duration of ~ 4 ms. The maximum energy measured from each pulse is approximately 20, 9, 6, and 4 MeV, respectively. Only the first pulse had an association with a sferic, which is different from the pattern reported by *Mezentsev et al.* [2016], who found that for all 16 multipulsed RHESSI TGFs with WWLLN associations, the association was simultaneous with the last peak. The number of sferics within a radius of 100 and 1000 km of the correlated TGF position and 10 min of the detection time was found to be 16 and 88, respectively, using the WWLLN data.

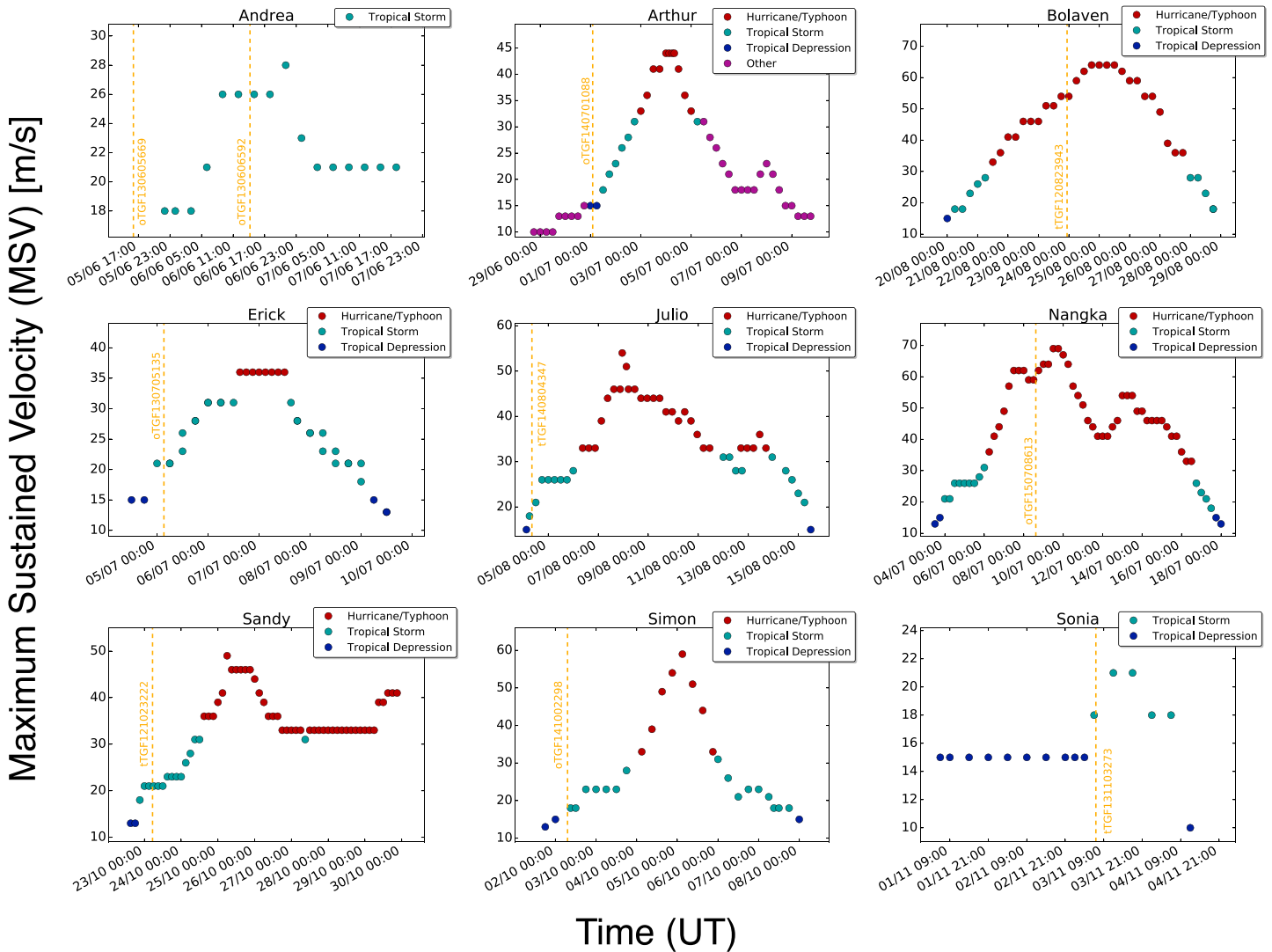


Figure 9. Storm histories of six weakening tropical storm systems, whose storm cells produced TGFs.

5.2.2. Tropical Storm Emang

Figure 13 is a satellite image of Tropical Storm Emang in the Southern Indian Ocean, taken by MTSAT on 15 January 2013. The storm was slowly intensifying over the open water in the days leading up to the TGF time, 1056 km from land. However, it encountered strong vertical wind shear, resulting in its dissipation on 17 January. Only nine strokes were detected by the WWLLN within 10 min and 1000 km of the TGF detection time. The energy distribution several milliseconds before and after the TGF trigger time reveals one event with a rapid rise time and a possible second pulse $\sim 250 \mu\text{s}$ after the first. The maximum energy detected by each pulse is approximately 5 and 2 MeV, respectively.

5.2.3. Tropical System Julio

A tropical wave formed off the coast of Mexico on 31 July 2014 and became increasingly organized, leading to the formation of a tropical depression at 03:00 UTC on the 4 August 2014. In the 24 h prior to this classification, four TGFs were detected by Fermi GBM, each with a VLF radio association. No TGFs were detected as the tropical depression rapidly strengthened into Tropical Storm Julio, 6 h after first being named, nor were any TGFs detected during the remainder of the storm's lifetime. oTGF140803355 occurred ~ 19 s before oTGF140803356, and oTGF140803425a occurred ~ 41 s before TGF140803425b. tTGF140804347 occurred approximately 26 h after oTGF140803425b. These TGF-producing storms are 117 km, 161 km, 372 km, 161 km, and 702 km away from the nearest landmass, respectively. Figure 14 shows satellite imagery data taken within an hour of the TGF detection times of oTGF140803355 and oTGF140803356, each overlaid with strokes detected by the ENTLN.

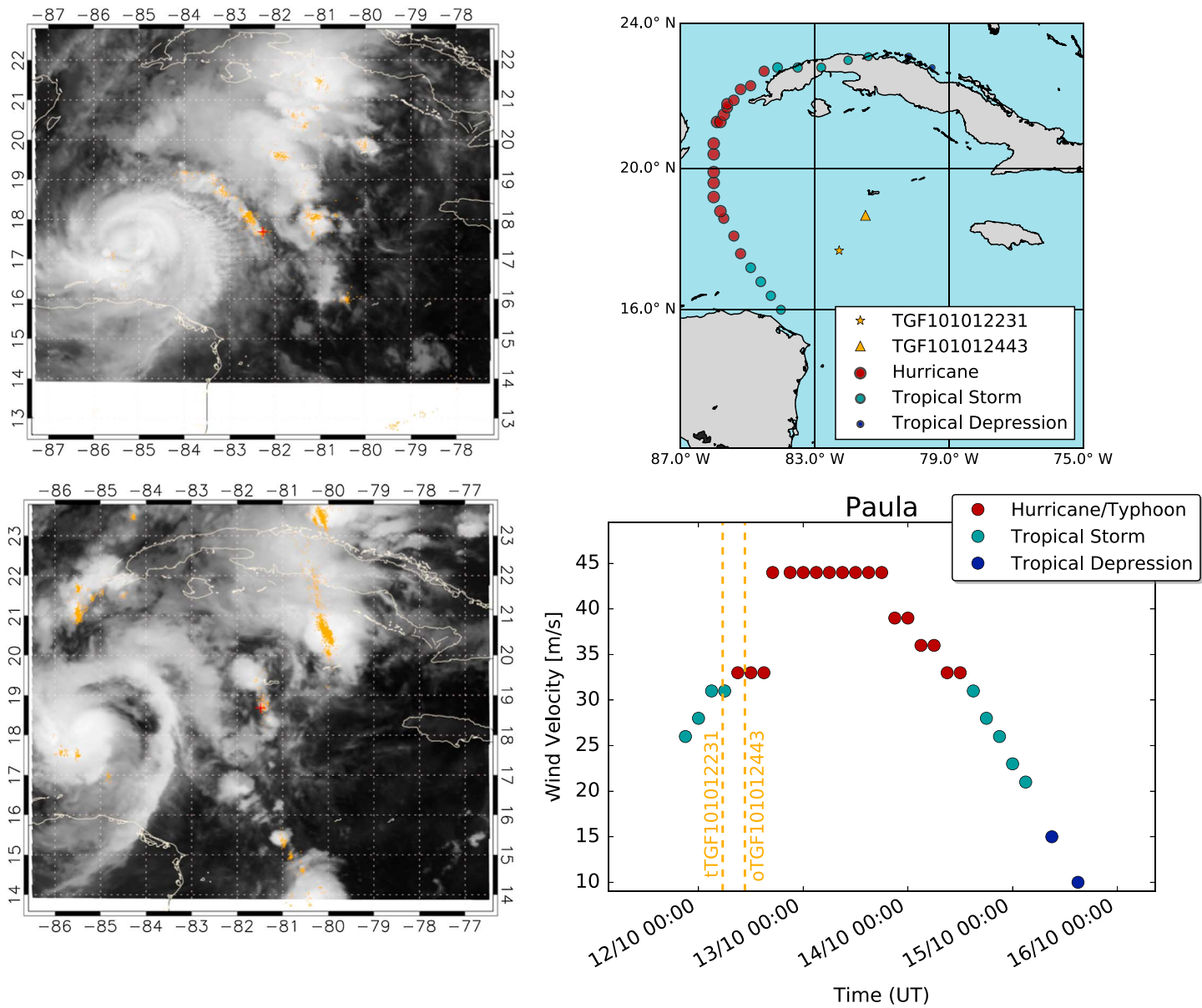


Figure 10. GOES images of Tropical Storm Paula as it strengthened into a Hurricane in the Gulf of Mexico. (top left) The first image shows the location of TGF101012231 with a red cross; (bottom left) the second image shows the location of TGF101012443. The images also show the sferics detected within 1000 km and 10 min (orange dots) of each TGF event. (right column) The storm track and intensity are shown. The dashed lines in the intensity plot (binned in daily intervals) shows the time of both TGFs during the history of the storm.

Like multipulsed events, oTGF140803425a and oTGF140803425b, oTGF140803355, and oTGF140803356 come from two separate storms. oTGF140803425a and oTGF140803425b are ~ 240 km apart, while oTGF140803355 and oTGF140803356 are only separated by ~ 70 km. The number of WWLLN sferics detected within 100 km and 10 min of oTGF140803355 was 127. Similarly, the number of WWLLN sferics within the same distance and time of oTGF140803356 was 116. In the 12 h following the last TGF (tTGF140804347) on 4 August, the storm rapidly intensified. During this period of intensification, the number of WWLLN sferics detected within 100 km and 10 min of tTGF140804347 was 521. The storm subsequently intensified further as atmospheric conditions became more favorable for storm development and became a category three Hurricane 4 days later. No TGFs with VLF associations were found after tTGF140804347 during these periods of the storm's lifetime.

These three storm systems are examples of intensifying tropical storm systems over open water. Typhoon Bolaven and Tropical Storm Emang are examples of storms with a low number of sferics around the TGF time. This is likely to be due to the weak updrafts typically observed from such tropical systems. The number of

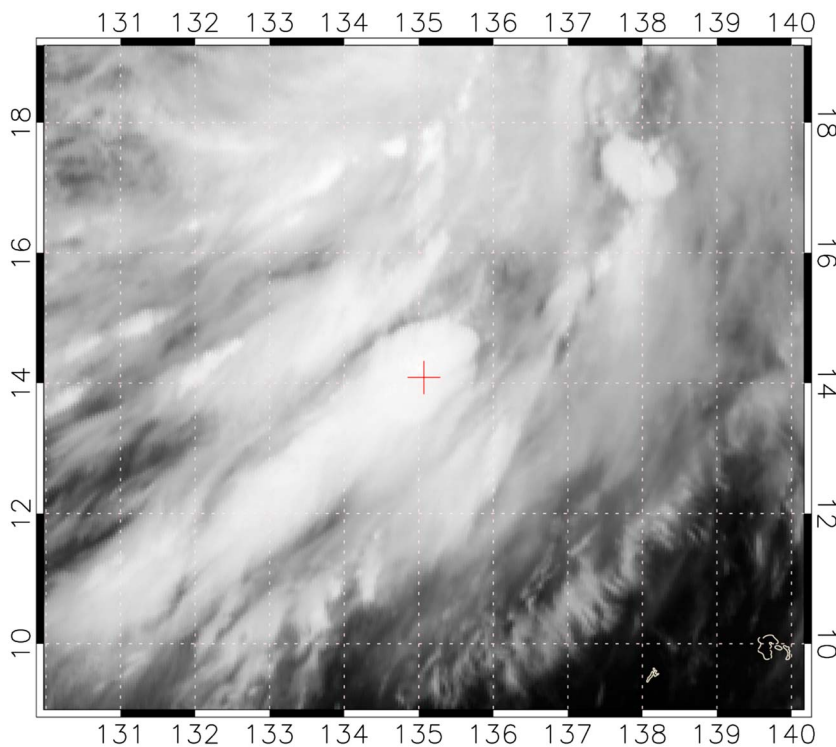


Figure 11. TGF120823943: The red cross represents the VLF source location (longitude: 135.07°E, latitude: +14.09°N), which was correlated with the GBM-detected TGF. The correlated TGF-VLF location was ~784 km from the center of Category 3 Typhoon Bolaven at the time of the TGF event.

WWLLN sferics associated with TGFs from Julio appeared to increase over 24 h. The storm system produced four TGFs within 100 min, each with an average of 200 sferics within 10 min and 1000 km of their respective associations. The cloud top temperatures and heights of three storm cells from Julio are given in Table 1. The cloud top heights of the storms that produced oTGF140803355 and oTGF140803356 were found to be 12.8 km and 15.3 km, respectively. tTGF140804347 is the last of five TGFs found in the Fermi GBM data from Julio, which came from a storm cell with a cloud top height of 15.9 km. 521 WWLLN sferics were observed within 100 km and 10 min of tTGF140804347, approximately 3 times higher than the number of sferics found within the same distance and time of the previous four TGF/WWLLN associations, detected 24 h earlier. Tropical Depression Julio was undergoing rapid intensification during this time, which corroborates with findings suggesting that

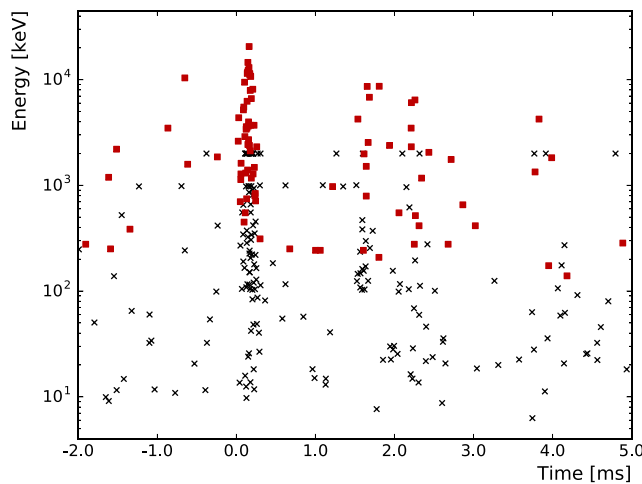


Figure 12. TGF120823943, which consists of four pulsed events over a 4 ms period. The maximum energy detected from the first pulse is 20 MeV and is the only one with an associated sferic.

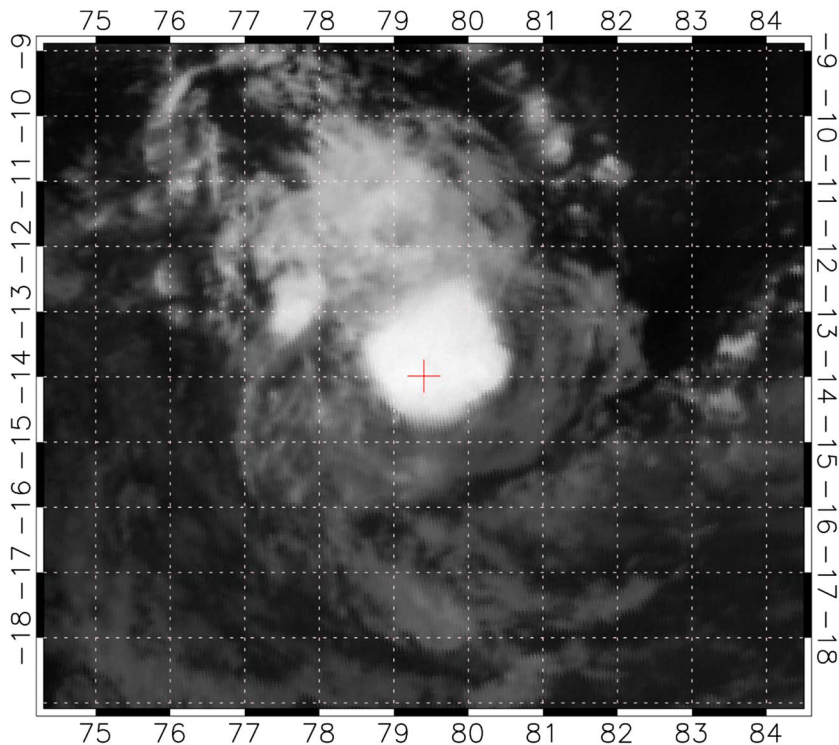


Figure 13. TGF130115502: The red cross represents the VLF source location (longitude: 79.53°E , latitude: -14.40°N), which was correlated with the GBM-detected TGF. The correlated TGF-VLF location was ~ 79 km from the center of Tropical Storm Emang at the time of the TGF event.

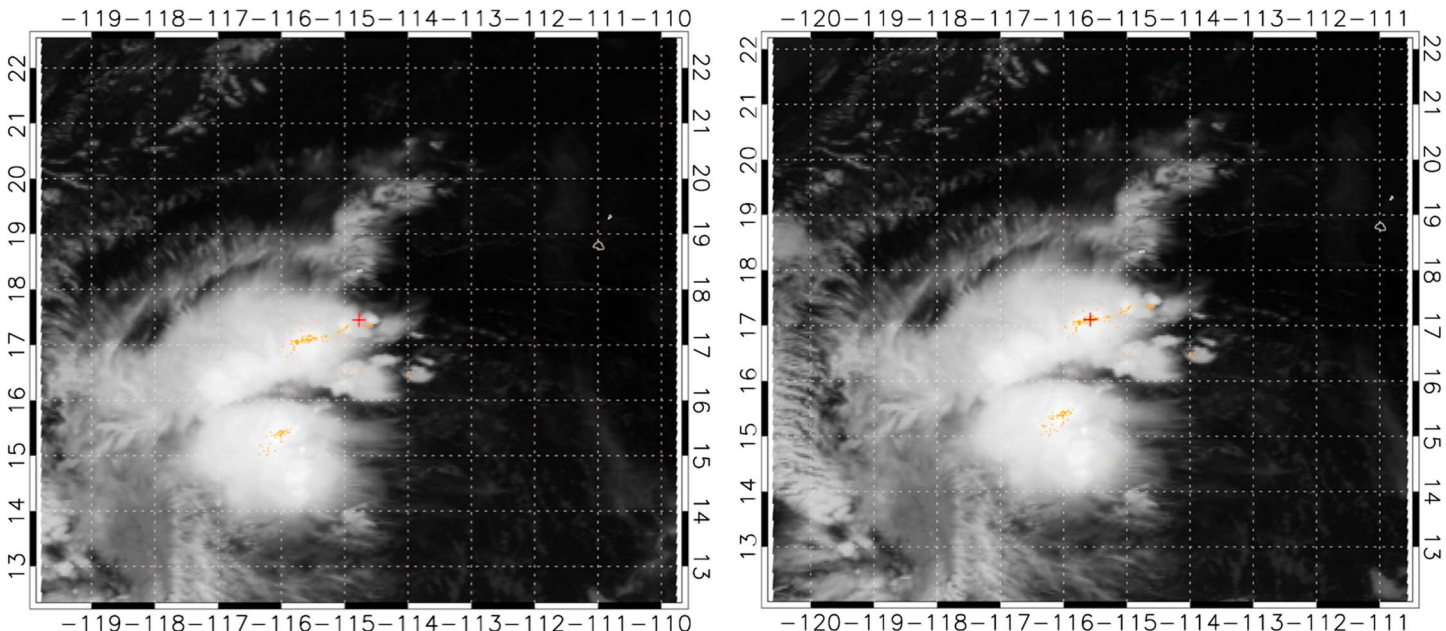


Figure 14. (left) TGF140803355: The red cross represents the VLF source location (longitude: 245.05°E , latitude: $+17.30^{\circ}\text{N}$), which was correlated with the GBM-detected TGF. (right) TGF140803356: The red cross represents the VLF source location (longitude: 244.42°E , latitude: $+17.11^{\circ}\text{N}$), which was correlated with the GBM-detected TGF. The orange dots in both satellite images represent the number of lightning strokes detected by the ENTLN within 10 min and 1000 km of each TGF.

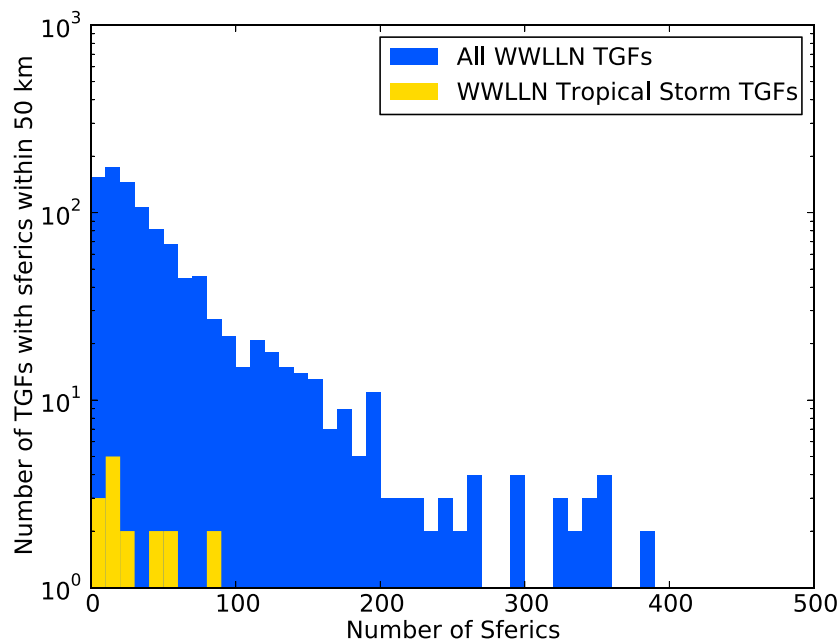


Figure 15. A plot showing the number of WWLLN Associated TGFs, with sferics within 50 km.

convective bursts and strengthening of updrafts are associated with an increase in highly energetic IC flashes. As the VLF networks are biased to high peak currents from IC lightning, the IC strokes responsible for these TGFs are likely to be a small fraction of the total lightning occurring in the storm, with a majority below the detection threshold of both VLF networks.

5.2.4. Storm Sferics

The three aforementioned storms are isolated from large continental land masses, lying hundreds of kilometers offshore. As the ionosphere and open ocean act as a near-perfect light guide for radio waves [Hutchins et al., 2012], the updraft strength of the encompassing storms is likely to be the main contributor to the low number of sferics observed for these three isolated storms.

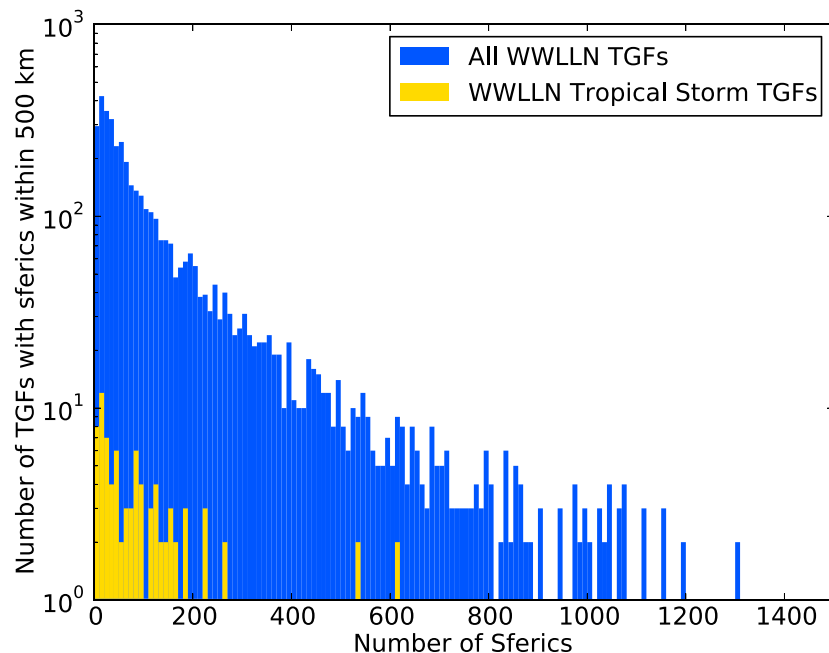


Figure 16. A plot showing the number of WWLLN Associated TGFs, with sferics within 500 km.

Analysis of the sferic data from WWLLN was performed in the following way. Of the TGFs in the GBM TGF catalog, those which have one or more WWLLN associations within ± 10 min were used. Additionally, TGFs with one or more WWLLN associations prior to 2010 were excluded as the WWLLN had lower detection efficiency and geographic uniformity, due to fewer stations. This resulted in a sample of 1049 TGFs with a VLF association and sferics within 1000 km. Of the 37 TGFs correlated to a storm in this sample, oTGF151010496 was excluded as it occurred outside the WWLLN-TGF catalog data. Of the remaining TGFs in the sample, 25 have a WWLLN association. The remaining 12 TGFs have an ENTLN association only.

Figures 15 and 16 show the number of TGFs with sferics within 50 km (Figure 15) and 500 km (Figure 16) of events taken from all TGFs with a WWLLN association up until 31 July 2015, which includes all but oTGF151010496 from the tropical storm sample. The data are tabulated such that there are 10 sferics/bin, which increment along the x axis. Figures 15 and 16 include TGF-producing storms during landfall as well as those out over the open ocean. Four TGF-producing storms were at distances greater than 500 km from land: oTGF120823943, oTGF130115502, oTGF131024758, and oTGF140804347. Three of these storms had a very low number of sferics within 10 min of each TGF-VLF event, some of which were discussed in detail previously. oTGF131024758 occurred in a storm approximately 77 km from the center of Tropical Storm Raymond in the Eastern Pacific Basin. Within 10 min on either side of this TGF-VLF association, there were only 41 and 43 sferics within 100 km and 300 km, respectively.

A small number of sferics occurring within a small distance of the TGF-VLF correlated event are expected, which is reflective of the activity in the individual and neighboring thunderstorm cells. As the radius is increased to 500 km, sferics from active storms further away or from a very extended storm become more prevalent. In this study, however, we find a subset of storms from our initial sample to have a small number of sferics. Although these sample sizes are small, it shows that lightning in low-sferic producing storms can still produce TGFs. For example, only nine sferics were detected by WWLLN at a location centred on oTGF130115502, within 10 min of the TGF-VLF simultaneous detection. The "TGF/sferic" ratio of this particular case is such that it may imply a high efficiency of TGF generation from lightning in this storm, where the lightning appears to be less frequent but stronger. There are several other previously mentioned cases of storms that appear to have this type of lightning, which might be expected as the IC+ association must have a peak current comparable or greater than CG lightning in order to be detected by the WWLLN. A comparative study of storms over the open ocean and land would help verify this result. Such a study is beyond the scope of this paper.

6. Conclusion

A sample of 37 Fermi-GBM TGFs with VLF correlations from tropical storm systems is presented for the first time. The sample spans the period from launch in June 2008 until the end of 2015. The properties of these TGFs were examined and compared with previous studies of the lightning rates in these macroscopic systems. It was found that the TGFs with VLF associations in this sample came predominately from tropical storm and tropical depression systems ($v_{\max} \leq 32 \text{ m s}^{-1}$). The locations of the TGF-producing storm cells in these types of systems were random in their distribution. Storm cells at the center of these tropical storm systems were just as likely to produce a TGF than those cells around the systems periphery. TGFs from typhoons or hurricanes ($v_{\max} \geq 32 \text{ m s}^{-1}$) came exclusively from the outer rainbands. This is expected, as previous studies [Cecil *et al.*, 2002; Cecil and Zipser, 2002] find that the highest lightning rates seem to occur in these regions of the storm many kilometers from the hostile environment of the storm center. No TGFs in this sample were found within 100–150 km of the eye wall region. Lightning in these regions is less likely than the outer rainbands but can occur under exceptional conditions (i.e., when a system is undergoing rapid intensification [Molinari *et al.*, 1999; Fierro *et al.*, 2011]). It is likely that TGFs from the inner rainband/eye wall regions do exist but that they are rarer than those TGFs produced in the outer rainbands, as the timing of the morphology of the storm and data acquisition is critical. Cloud top heights were estimated using sounding data and data from the GOES images for 23 storm cells in this sample. The warmest temperatures recorded from the images were around -50°C , corresponding to a cloud top height of ~ 9.7 km. The highest cloud top heights found in this data are likely to be from very cold, overshooting cloud tops with altitudes of ≥ 17 km.

The observed gamma ray properties of the TGFs such as their hardness ratio (HR) and duration were calculated and compared to the larger GBM catalog sample. No deviations between both data sets were observed. The duration for all the TGFs in this sample were found to be shorter than the average TGF. However, as this

sample exclusively uses TGFs with VLF associations, the duration is biased to shorter TGFs and is not likely to be representative of TGFs from tropical storms. TGFs without associations that can be conclusively associated to a temporally coincident storm system will help determine the true duration distribution of TGFs from tropical storms.

This study has shown that of the 37 TGFs in our sample, 25 occurred during the strengthening phase of a tropical storm system, eight occur during the dissipation stage, and four during the peak intensity of the tropical storm. These tropical storm systems occur along the seasonally dependent track of the ITCZ and result in a non-negligible contribution of oceanic TGFs. Although the data in this study indicates a correlation of TGF activity with storm phase, a TGF from a strengthening tropical depression does not mean that that system will become an especially violent storm later in its lifetime. It only suggests that the likelihood of TGF detection by GBM is greater at these epochs, as convective bursts and strengthening updrafts are associated with an increase in the discharge heights of highly energetic IC flashes, which have peak currents comparable to CG lightning, and therefore are present in the sferic association data.

A case study presented five TGFs that occurred over a 24 h period from storm system Julio. The first four TGFs occurred within 100 min of each other, from storm cells containing approximately 100 sferics within 100 km and 10 min of their associations. However, tTGF140804347 (which occurred 24 h after the first four TGFs) was found to originate from a storm cell that had three times the number of sferics. The tropical depression was undergoing rapid intensification at the time of tTGF140804347, which corroborates with findings suggesting that convective bursts and strengthening of updrafts are associated with an increase in highly energetic IC flashes.

Another case study showed a TGF from the outer rainband of Typhoon Bolaven, which intensified to become a super typhoon 18 h later. This TGF had an association from both the ENTLN and WWLLN data and consisted of multiple pulses over a 4 ms period, with energy extending up to 20 MeV. The number of sferics from both networks showed little activity over a 10 min period, within 1000 km of the VLF association. Similarly, another case study showed a TGF from the center of a deep area of convection associated with Tropical Storm Emang in the middle of the Indian Ocean. The number of sferics from the WWLLN data for this storm only showed nine sferics over a 10 min period, within 1000 km of the VLF sferic associated with oTGF130115502. The low number of sferics in these case studies is expected due to the fact that storm systems over the open ocean have weaker updrafts than those over land, in general agreement with studies by Black *et al.*, [1996] and Black and Hallett, [1999]. Due to the updrafts being so weak and the freezing levels so high, very little supercooled droplets are permeating into the charge layer regions of the storm clouds. The ratio of sferics to TGFs for these extraordinary cases may imply these storms are more efficient at generating TGFs, as the lightning appears to be less frequent but stronger. This might be expected as the IC+ association must have a peak current comparable or greater than CG lightning in order to be detected by the WWLLN. The finding that even such weak storms are capable of producing TGFs is in keeping with the conclusions drawn from Chronis *et al.* [2015], although further investigation into such storms is required.

The continuing addition of ground transceiver stations to the ENTLN and the WWLLN will increase the detection efficiency of sferics from TGFs many miles from land, where tropical storm systems predominately occur and strengthen. The GOES-16 Global Lightning Mapping (GLM) instrument will allow for correlations of lightning to satellite imagery, which can be used in future pipelines allowing TGFs to be detected nearly simultaneously with the satellite and lightning data images. Such a tool would be extremely useful in expanding the TGF tropical storm sample and in confirming our findings.

References

- Abarca, S. F., K. L. Corbosiero, and T. J. Galarneau Jr. (2010), An evaluation of the World Wide Lightning Location Network (WWLLN) using the National Lightning Detection Network (NLDN) as ground truth, *J. Geophys. Res.*, 115, D18206, doi:10.1029/2009JD013411.
- Atwood, W. B., et al. (2009), The Large Area Telescope on the Fermi Gamma-ray Space Telescope mission, *Astrophys. J.*, 697, 1071–1102.
- Babich, L. P., E. I. Bochkov, I. M. Kutsyk, T. Neubert, and O. Chanrion (2015), A model for electric field enhancement in lightning leader tips to levels allowing X-ray and γ ray emissions, *J. Geophys. Res. Space Physics*, 120(6), 5087–5100, doi:10.1002/2014JA020923.
- Bedka, K. M., C. Wang, R. Rogers, L. Carey, W. Feltz, and J. Kanak (2015), Examining deep convective cloud evolution using total lightning, WSR-88D, and GOES-14 Super Rapid Scan datasets, *Weather Forecasting*, 30, 571–590.
- Bessho, K., et al. (2016), An introduction to Himawari-8/9—Japan's new-generation geostationary meteorological satellites, *J. Meteorol. Soc. Jpn. II*, 94(2), 151–183.
- Black, M. L., R. W. Burpee, and F. D. Marks Jr. (1996), Vertical motion characteristics of tropical cyclones determined with airborne Doppler radial velocities, *J. Atmos. Sci.*, 53, 1887–1909.
- Black, R. A., and J. Hallett (1999), Electrification of the hurricane, *J. Atmos. Sci.*, 56, 2004–2028.

Acknowledgments

The Fermi GBM Collaboration acknowledges the support of NASA in the United States and DLR in Germany. We thank NASA for support from Fermi Guest Investigation NNX13AO89G. O.J.R. acknowledges support from Science Foundation Ireland under grant 12/IP/1288. E.C. acknowledges NSF support, grant 1524533. The authors wish to thank the World Wide Lightning Location Network (<http://wwlln.net>), a collaboration among over 50 universities and institutions, for providing the lightning location data used in this paper. We also acknowledge Earth Networks for providing the ENTLN data used in this study. All the GBM and WWLLN data used in this paper are available from the FSSC catalog <https://fermi.gsfc.nasa.gov/ssc/data/access/gbm/tgf/>. ENTLN localizations for these TGFs can be made available from the author. The tropical storm data are available from <http://weather.unisys.com/hurricane/index.php>. The meteorological image data are available from <http://www.ncdc.noaa.gov/gibbs/> and <http://inventory.ssec.wisc.edu/inventory/>. The storm track information is taken from the National Oceanic and Atmospheric Administration (NOAA) data (<http://www.nhc.noaa.gov/data/>), Weather Underground's Hurricane Archive (<https://www.wunderground.com/hurricane/hurarchive.asp>) and the UniSys archive (<http://weather.unisys.com/hurricane/>).

- Blakeslee, R. J., D. M. Mach, M. G. Bateman, and J. C. Bailey (2014), Seasonal variations in the lightning diurnal cycle and implications for the global electric circuit, *Atmos. Res.*, 135–136, 228–243, doi:10.1016/j.atmosres.2012.09.023.
- Bovalo, C., C. Barthe, N. Yu, and N. Bègue (2014), Lightning activity within tropical cyclones in the South West Indian Ocean, *J. Geophys. Res. Atmos.*, 119, 8231–8244, doi:10.1002/2014JD021651.
- Briggs, M. S., et al. (2010), First results on terrestrial gamma ray flashes from the Fermi Gamma-ray Burst Monitor, *J. Geophys. Res.*, 115, A07323, doi:10.1029/2009JA015242.
- Briggs, M. S., et al. (2013), Terrestrial gamma-ray flashes in the Fermi era: Improved observations and analysis methods, *J. Geophys. Res. Space Physics*, 118, 3805–3830, doi:10.1002/jgra.50205.
- Bui, V. Y., L.-C. Chang, and S. Heckman (2015), A Performance Study of Earth Networks Total Lighting Network (ENTLN) and Worldwide Lightning Location Network (WWLLN), in *Proceeding IEEE 2015 International Conference on Computational Science and Computational Intelligence (CSCI)*, pp. 386–391, IEEE Computer Society, Washington, D. C., doi:10.1109/CSCI.2015.120.
- Carlson, B. E., N. G. Lehtinen, and U. S. Inan (2007), Constraints on terrestrial gamma ray flash production from satellite observation, *Geophys. Res. Lett.*, 34, L08809, doi:10.1029/2006GL029229.
- Cecil, D. J., and E. J. Zipser (2002), Reflectivity, ice scattering, and lightning characteristics of hurricane eyewalls and rainbands. Part II: Intercomparison of observations, *Mon. Weather Rev.*, 130, 769–784.
- Cecil, D. J., E. J. Zipser, and S. W. Nesbitt (2002), Reflectivity, ice scattering, and lightning characteristics of hurricane eyewalls and rainbands. Part I: Quantitative description, *Mon. Weather Rev.*, 130, 769–784.
- Celestin, S., and V. P. Pasko (2011), Energy and fluxes of thermal runaway electrons produced by exponential growth of streamers during the stepping of lightning leaders and in transient luminous events, *J. Geophys. Res.*, 116, A03315, doi:10.1029/2010JA016260.
- Chen, S. M., Y. Du, and L. M. Fan (2004), Lightning data observed with lightning location system in Guangdong Province, China, *IEEE Trans. Power Delivery*, 19(3), 1148–1153.
- Christian, H. J., et al. (2003), Global frequency and distribution of lightning as observed from space by the Optical Transient Detector, *J. Geophys. Res.*, 108(D1), 4005, doi:10.1029/2002JD002347.
- Chronis, T., M. S. Briggs, G. Priftis, V. Connaughton, J. Brundell, R. Holzworth, S. Heckman, S. McBreen, Fitzpatrick G., and M. Stanbro (2015), Characteristics of thunderstorms that produce terrestrial gamma-ray flashes, *Bull. Am. Meteorol. Soc.*, doi:10.1175/BAMS-D-14-00239.1.
- Cohen, M. B., U. S. Inan, and G. Fishman (2006), Terrestrial gamma ray flashes observed aboard the Compton Gamma Ray Observatory/Burst and Transient Source Experiment and ELF/VLF radio atmospherics, *J. Geophys. Res.*, 111, D24109, doi:10.1029/2005JD006987.
- Collier, A. B., T. Gjesteland, and N. Østgaard (2011), Assessing the power law distribution of TGFs, *J. Geophys. Res.*, 116, 2156–2202, doi:10.1029/2011JA016612.
- Connaughton, V., et al. (2010), Associations between Fermi Gamma-ray Burst Monitor terrestrial gamma ray flashes and sferics from the World Wide Lightning Location Network, *J. Geophys. Res.*, 115, A12307, doi:10.1029/2010JA015681.
- Connaughton, V., et al. (2013), Radio signals from electron beams in terrestrial gamma ray flashes, *J. Geophys. Res. Space Physics*, 118, 2313–2320, doi:10.1029/2012JA018288.
- Cummer, S. A., Y. Zhai, W. Hu, D. M. Smith, L. I. Lopez, and M. A. Stanley (2005), Measurements and implications of the relationship between lightning and terrestrial gamma ray flashes, *Geophys. Res. Lett.*, 32, L08811, doi:10.1029/2005GL022778.
- Cummer, S. A., G. Lu, M. S. Briggs, V. Connaughton, S. Xiong, G. J. Fishman, and J. R. Dwyer (2011), The lightning-TGF relationship on microsecond timescales, *Geophys. Res. Lett.*, 38, L14810, doi:10.1029/2011GL048099.
- De Maria, M., R. T. De Maria, J. A. Knaff, and D. Molenar (2012), Tropical cyclone lightning and rapid intensity change, *Mon. Weather Rev.*, 140, 1828–1842, doi:10.1175/MWR-D-11-00236.1.
- Dowden, R. L., J. B. Brundell, and C. J. Rodger (2002), VLF lightning location by time of group arrival (TOGA) at multiple sites, *J. Atmos. Sol. Terr. Phys.*, 64, 817–830.
- Dwyer, J. R. (2008), The source mechanisms of terrestrial gamma-ray flashes, *J. Geophys. Res.*, 113, D10103, doi:10.1029/2007JD009248.
- Dwyer, J. R. (2012), The relativistic feedback discharge model of terrestrial gamma ray flashes, *J. Geophys. Res.*, 117, A02308, doi:10.1029/2011JA017160.
- Dwyer, J. R., and S. A. Cummer (2013), Radio emissions from terrestrial gamma-ray flashes, *J. Geophys. Res. Space Physics*, 118, 3769–3790, doi:10.1002/jgra.50188.
- Dwyer, J. R., and D. M. Smith (2005), A comparison between Monte Carlo simulations of runaway breakdown and terrestrial gamma-ray flash observations, *Geophys. Res. Lett.*, 32, L22804, doi:10.1029/2005GL023848.
- Dwyer, J. R., D. M. Smith, and S. A. Cummer (2012), High-energy atmospheric physics: Terrestrial gamma-ray flashes and related phenomena, *Space Sci. Rev.*, 173, 133–196, doi:10.1007/s11214-012-9894-0.
- Fabró, F., J. Montanyà, M. Marisaldi, O. A. van der Velde, and F. Fuschino (2015), Analysis of global Terrestrial Gamma Ray Flashes distribution and special focus on AGILE detections over South America, *J. Atmos. Sol. Terr. Phys.*, 124, 10–20, doi:10.1016/j.jastp.2015.01.009.
- Fierro, A. O., X.-M. Shao, T. Hamlin, J. M. Reisner, and J. Harlin (2011), Evolution of eyewall convective events as indicated by intracloud and cloud-to-ground lightning activity during the rapid intensification of Hurricanes Rita and Katrina, *Mon. Weather Rev.*, 139, 1492–1504.
- Fishman, G. J., et al. (1994), Discovery of intense gamma-ray flashes of atmospheric origin, *Science*, 264, 1313–1351.
- Fitzpatrick, G., et al. (2014), Compton scattering in terrestrial gamma-ray flashes detected with the Fermi gamma-ray burst monitor, *Phys. Rev. D*, 90, 043008.
- Fitzpatrick, P. J. (2006), *Hurricanes: A Reference Handbook*, Contemporary World Issues, 2nd ed., 23 pp., ABC-CLIO, Inc., Santa Barbara, Calif.
- Foley, S., et al. (2014), Pulse properties of terrestrial gamma-ray flashes detected by the Fermi gamma-ray burst monitor, *J. Geophys. Res. Space Physics*, 119, 5931–5942, doi:10.1029/2014JA019805.
- Gjesteland, T., N. Østgaard, P. H. Connell, Stadsnes J., and G. J. Fishman (2010), Effects of dead time losses on terrestrial gamma ray flash measurements with the burst and transient source experiment, *J. Geophys. Res.*, 115, A00E21, doi:10.1029/2009JA014578.
- Gjesteland, T., N. Østgaard, S. Laviola, M. M. Miglietta, E. Arnone, M. Marisaldi, F. Fuschino, A. B. Collier, F. Fabró, and J. Montanya (2015), Observation of intrinsically bright terrestrial gamma ray flashes from the Mediterranean basin, *J. Geophys. Res. Atmos.*, 120, 12,143–12,156, doi:10.1002/2015JD023704.
- Grefenstette, B. W., D. M. Smith, J. R. Dwyer, and G. J. Fishman (2008), Time evolution of terrestrial gamma ray flashes, *Geophys. Res. Lett.*, 35, L06802, doi:10.1029/2007GL032922.
- Grefenstette, B. W., D. M. Smith, B. J. Hazelton, and L. I. Lopez (2009), First RHESSI terrestrial gamma ray flash catalog, *J. Geophys. Res.*, 114, A02314, doi:10.1029/2008JA013721.
- Grove, J. E., A. Chekhtman, Fermi LAT Collaboration, G. Fishman, M. Briggs, Connaughton V., and Fermi-GBM Collaboration (2012), Observation of terrestrial gamma-ray flashes with Fermi LAT, *American Astronomical Society Meeting Abstracts* 219, 149.13.
- Hutchins, M. L., R. H. Holzworth, J. B. Brundell, and C. J. Rodger (2012), Relative detection efficiency of the World Wide Lightning Location Network, *Radio Sci.*, 47, RS6005, doi:10.1029/2012RS005049.

- Hutchins, M. L., R. H. Holzworth, K. S. Virts, J. M. Wallace, and S. Heckman (2013), Radiated VLF energy differences of land and oceanic lightning, *Geophys. Res. Lett.*, **40**, 2390–2394, doi:10.1002/grl.50406.
- Hutchins, M. L., R. H. Holzworth, and J. B. Brundell (2014), Diurnal variation of the global electric circuit from clustered thunderstorms, *J. Geophys. Res. Space Physics*, **119**, 620–629, doi:10.1002/2013JA019593.
- Inan, U. S., M. B. Cohen, R. K. Said, D. M. Smith, and L. I. Lopez (1996), Terrestrial gamma ray flashes and lightning discharges, *Geophys. Res. Lett.*, **33**, L18802, doi:10.1029/2006GL027085.
- Jacobson, A. R., R. Holzworth, J. Harlin, R. Dowden, and E. Lay (2006), Performance assessment of the World Wide Lightning Location Network (WWLLN), using the Los Alamos Sferic Array (LASA) as ground truth, *J. Atmos. Oceanic Technol.*, **23**, 1082–1092.
- Lay, E. H., R. H. Holzworth, C. J. Rodger, J. N. Thomas, O. Pinto, and R. L. Dowden (2004), WWLLN global lightning detection system: Regional validation study in Brazil, *Geophys. Res. Lett.*, **31**, L03102, doi:10.1029/2003GL018882.
- Liu, C., and S. Heckman (2011), The application of total lightning detection and cell tracking for severe weather prediction, in *91st American Meteorological Society Annual Meeting*, pp. 1–10, Seattle, Wash.
- Mailyan, B. G., M. S. Briggs, E. S. Cramer, G. Fitzpatrick, O. J. Roberts, M. Stanbro, V. Connaughton, S. McBreen, P. N. Bhat, and J. R. Dwyer (2016), The spectroscopy of individual terrestrial gamma-ray flashes: Constraining the source properties, *J. Geophys. Res. Space Physics*, **121**, 11,346–11,363, doi:10.1002/2016JA022702.
- Marisaldi, M., et al. (2014), Properties of terrestrial gamma-ray flashes detected by AGILE MCAL below 30 MeV, *J. Geophys. Res. Space Physics*, **119**, 1337–1355, doi:10.1002/2013JA019301.
- Meegan, C., et al. (2009), The Fermi gamma-ray burst monitor, *Astrophys. J.*, **702**, 791–804.
- Mezentsev, A., N. Østgaard, T. Gjesteland, K. Albrechtsen, N. Lehtinen, M. Marisaldi, D. Smith, and S. Cummer (2016), Radio emissions from double RHESSI TGFs, *J. Geophys. Res. Atmos.*, **121**, 8006–8022, doi:10.1002/2016JD025111.
- Molinari, J., P. Moore, and V. Idone (1999), Convective structure of hurricanes as revealed by lightning locations, *Mon. Weather Rev.*, **127**, 520–534.
- Moss, G. D., V. P. Pasko, N. Liu, and G. Veronis (2006), Monte Carlo model for analysis of thermal runaway electrons in streamer tips in transient luminous events and streamer zones of lightning leaders, *J. Geophys. Res.*, **111**, A02307, doi:10.1029/2005JA011350.
- Nagele, D. (2010), Analysis of cloud-to-ground lightning within tropical cyclones, MS thesis, 89 pp., Texas Tech Univ., Lubbock.
- Østgaard, N., T. Gjesteland, J. Stadsnes, P. H. Connell, and B. Carlson (2008), Production altitude and time delays of the terrestrial gamma flashes: Revisiting the Burst and Transient Source Experiment spectra, *J. Geophys. Res.*, **113**, A02307, doi:10.1029/2007JA012618.
- Price, C. (2008), Lightning sensors for observing, tracking and nowcasting severe weather, *Sensors*, **8**, 157–170.
- Price, J. F. (2009), Metrics of hurricane-ocean interaction: Vertically-integrated or vertically-averaged ocean temperature?, *Ocean Sci.*, **5**, 351–368.
- Puschell, J. J., H. A. Lowe, J. Jeter, S. Kus, W. Todd Hurt, D. Gilman, D. Rogers, and R. Hoelter (2002), *Japanese Advanced Meteorological Imager: A Next Generation GEO Imager for MTSAT-1R*, Proceedings of SPIE 4814, Earth Observing Systems VII, 152, Seattle, Wash.
- Rodger, C. J., J. B. Brundell, and R. L. Dowden (2005), Location accuracy of VLF World Wide Lightning Location (WWLL) network: Post-algorithm upgrade, *Ann. Geophys.*, **23**, 277–290.
- Rodger, C. J., S. Werner, J. B. Brundell, E. H. Lay, N. R. Thomson, R. H. Holzworth, and R. L. Dowden (2006), Detection efficiency of the VLF World-Wide Lightning Location Network (WWLLN): Initial case study, *Ann. Geophys.*, **24**, 3197–3214.
- Rodger, C. J., J. B. Brundell, R. H. Holzworth, and E. H. Lay (2008), Growing detection efficiency of the World Wide Lightning Location Network, in *Proceedings Conference on Coupling of Thunderstorms and Lightning Discharges to Near-Earth Space*, vol. 1118, pp. 15–20, American Institute of Physics, Corte, France.
- Rudlosky, S. D. (2015), Evaluating ENTLN performance relative to TRMM/LIS, *J. Oper. Meteorol.*, **3**(2), 11–20, doi:10.15191/nwajom.2015.0302.
- Said, R. K., M. B. Cohen, and U. S. Inan (2013), Highly intense lightning over the oceans: Estimated peak currents from global GLD360 observations, *J. Geophys. Res. Atmos.*, **118**, 6905–6915, doi:10.1002/jgrd.50508.
- Scargle, J. D., J. P. Norris, B. Jackson, and J. Chiang (2013), Studies in astronomical time series analysis. VI. Bayesian block representations, *Astrophys. J.*, **764**, 167.
- Seity, Y., S. Soula, and H. Sauvageot (2001), Lightning and precipitation activities in coastal thunderstorms, *J. Geophys. Res. Atmos.*, **106**(D19), 22,801–22,816.
- Shao, X.-M., M. Stanley, A. Regan, J. Harlin, M. Pongratz, and M. Stock (2006), Total lightning observations with the new and improved Los Alamos Sferic Array (LASA), *J. Atmos. Oceanic Technol.*, **23**, 1273–1288.
- Smith, D. M., L. I. Lopez, R. P. Lin, and C. P. Barrington-Leigh (2005), Terrestrial gamma-ray flashes observed up to 20 MeV, *Science*, **307**, 1085–1088, doi:10.1126/science.1107466.
- Split, M. E., S. M. Lazarus, D. Barnes, J. R. Dwyer, H. K. Rassoul, D. M. Smith, B. Hazelton, and B. Grefenstette (2010), Thunderstorm characteristics associated with RHESSI identified terrestrial gamma ray flashes, *J. Geophys. Res.*, **115**, 2156–2202.
- Stanley, M. A., X.-M. Shao, D. M. Smith, L. I. Lopez, M. B. Pongratz, J. D. Harlin, M. Stock, and A. Regan (2006), A link between terrestrial gamma-ray flashes and intracloud lightning discharges, *Geophys. Res. Lett.*, **33**, L06803, doi:10.1029/2005GL025537.
- Tavani, M., et al. (2011), Terrestrial gamma-ray flashes as powerful particle accelerators, *Phys. Rev. Lett.*, **106**(1), 01850.
- Tierney, D., et al. (2013), Fluence distribution of terrestrial gamma ray flashes observed by the Fermi Gamma-ray Burst Monitor, *J. Geophys. Res. Space Physics*, **118**, 6644–6650.
- Uesawa, D. (2006), Status of Japanese meteorological satellites and recent activities of MSC, in *Proceedings of the 2006 EUMETSAT Meteorological Satellite Conference*, Meteorological Satellite Center, Japan Meteorological Agency, Helsinki, Finland.
- Virts, K. S., J. M. Wallace, M. L. Hutchins, and R. Holzworth (2013), Highlights of a new ground-based, hourly global lightning climatology, *Bull. Am. Meteorol. Soc.*, **1381**–1391, doi:10.1175/BAMS-D-12-00082.1.
- Wiens, K. C., S. A. Rutledge, and S. A. Tessendorf (2005), The 29 June 2000 supercell observed during STEPS. Part II: Lightning and charge structure, *J. Atmos. Sci.*, **62**, 4151–4177.
- Williams, E., et al. (2006), Lightning flashes conducive to the production and escape of gamma radiation to space, *J. Geophys. Res.*, **111**, D16209, doi:10.1029/2005JD006447.
- Zhang, W., Y. Zhang, D. Zheng, and X. Zhou (2012), Lightning distribution and eyewall outbreaks in tropical cyclones during landfall, *Mon. Weather Rev.*, **140**, 3573–3586.